Response to the reviewers

We thank the reviewers for their thoughtful and constructive review of our manuscript. In the following we address their concerns and suggestions point by point.

Reviewer 1

Summary: The authors present a new landscape evolution model, HyLands, that combines models of landsliding and bedrock evolution. The backbone of the model, SPACE by Shobe et al. 2017, can shift between both transport-limited and detachment-limited cases of landscape evolution and therefore simulate the continuum of bedrock to mixed bedrock-alluvial to alluvial rivers. Here, bedrock erosion is modulated by the cover effect, which greatly depends on the rate that sediment is delivered to the channel. HyLands combines SPACE with a landsliding model that allows for sediment delivery in a highly punctuated fashion instead of a steady rate. The authors first demonstrate the steady-state solutions for the SPACE model in the Topo Toolbox. Landscape Evolution Model (TTLEM) framework. They then add landsliding to a natural landscape (Namche-Barwa region) and found that the modeled and observed characteristics of the landslide dynamics match quite well. Last, they devise a model run on a synthetic landscape where there is a 100-year period of intense landsliding to simulate widespread co-seismic landslides. They found that landslides create drainage rerouting from landslide blockage and generate channel knickpoints. They conclude by discussing calibration techniques and potential applications for HyLands.

Review: This manuscript is well written and contains a detailed description of the numerical model, HyLands. The literature review covers the field of numerical landscape evolution modeling and makes a compelling argument for why a model like HyLands is needed. The objectives and motivation are well-thought out and are clear to the reader. The discussion is thorough, and I appreciate the effort the authors took to flesh out potential calibration techniques and applications to their model. They conclude by stating that their model is "well-suited to address a range of new questions related to how channel-hillslope coupling modulates landscape response," which I wholeheartedly believe. However, I think this manuscript should take a more in-depth look at the steady-state behavior of this model. I believe this manuscript should be accepted with some minor revisions.

Verification:

The manuscript shows steady-state solutions for detachment-limited, transport-limited,and mixed bedrock-alluvial cases. These solutions and the associate figure are quite similar to the work in Shobe et al., 2017, and I am not sure it is totally necessary for them to be repeated in this manuscript. Figure 8 shows HyLands working remarkably well compared to the data of Larsen and Montgomery, 2012, but it seems that the model systematically overestimates landslide volumes for all scales of landslides. The author's attribute the overestimation of small landslide volumes to the inability of the model to deposit materials in the landslide scars. What is the reasoning for the model overestimating large landslide volumes?

Synthetic Landscapes:

At what spatial scale is the drainage re-routing occurring? From Figure 9 (d, e, and f) and Figure 10, it does not seem that the channel profile's location has changed significantly. The figures make it seem like the channel moves on the order of one cell size due to valley blockage and the formation of epigenetic gorges. Could these slight reorganizations, over long periods, create major drainage reorganization or river piracy? Related, how computationally expensive is the landslide (non-linear deposition) routing compared to the rest of the model? I'm really excited for researchers to start using this model. I would be interested to know how fast the model runs, and how modifications that complicate or simplify the landsliding component of HyLands would affect the computational efficiency.The first part of the model verification section details the steady-state behavior of detachment-limited, transport-limited, and mixed bedrock-alluvial landscapes. I would like authors to answer: **How does the steady state behavior of a mixed bedrock-alluvial landscape with landslides as the sediment delivery mechanism compare to a simulation without landslides?** My guess would be that the main controlling parameter would be t_{LS}, the return time for landsliding. For very small values of t_{LS}, small frequent landslides will dominate; however, there will be little time for the landscape to recover/build up storage of landslide material. In this case, I believe the model would act very similarly to the initial runs in SPACE. For large t_{LS} values, large but seldom landslides dominate. If the landslides are very rare, I think the landscapes will also act similarly to SPACE. In between these two extremes, I think there is potential for the landscape to behave quite differently. Please consider reading Zhang et al., 2018 (The Advective-Diffusive Morphodynamics of Mixed Bedrock-Alluvial Rivers Subjected to Spatiotemporally Varying Sediment Supply) paper which also considers the tool effect.

Reply: We explicitly want to thank reviewer 1, to review our manuscript in such a short period, given the challenging times. We are pleased that the reviewer appreciates our work and agrees on the need for the development of LEMs like HyLands. In the following, we address her/his specific comments.

RC 1.1 — The manuscript shows steady-state solutions for detachment-limited, transport-limited,and mixed bedrock-alluvial cases. These solutions and the associate figure are quite similar to the work in Shobe et al., 2017, and I am not sure it is totally necessary for them to be repeated in this manuscript.

Reply: We indeed reproduced the analytical verification methods for SPACE as earlier proposed by Shobe et al., 2017. We also considered moving this part to a supplementary file but decided to keep in in the main body of the text because of the following. Space has been developed and tested in the Landlab framework. We ported the same set of equations to the TTLEM modelling environment. To validate our implementation we tested it thoroughly by comparing model output with these well established sets of analytical fluvial equations. While this is not new from a scientific point of view, we believe it is important for every new numerical model to be tested rigorously against such benchmark equations. Given the scope of the GMD journal, we therefore decided to report on these comparisons and keep the fluvial model verification exercise in the main text of the manuscript. Moreover, the set of model runs we use here, is used at a later stage in the paper to show the impact of landslides on fluvial sediment dynamics. Showing the functionally of the fluvial component is therefore key to support our findings documented at a later stage in this paper.

RC 1.2 — Figure 8 shows HyLands working remarkably well compared to the data of Larsen and Montgomery, 2012, but it seems that the model systematically overestimates landslide volumes for all scales of landslides. The author's attribute the overestimation of small landslide volumes to the inability of the model to deposit materials in the landslide scars. What is the reasoning for the model overestimating large landslide volumes?

Reply: This is a valid point. As we explicitly mention in section 3.2.2, we use the Namche-Barwa area solely to demonstrate and evaluate the performance of HyLands. We do not take into account a number of boundary conditions (such as uplift patterns, see section 3.2.2) which prevents us to reproduce exact features of landscape exhumation in this region. Therefore, we ran the model with standard parameters values and did not calibrate any of them (see also RC 1.5). We evaluated the the performance of the landslide algorithm against its capability of reproducing the shape of empirical universal magnitude-frequency and area-volume relationships. We did not aim to exactly reproduce the observed scaling relationships since this would involve calibration and uncertainty analysis of the model, which is beyond the scope of this paper. Regarding the Area-Volume relationship in particular, what we see is that the volume of small landslides deviates from the otherwise linear Area-Volume relationship (in a loglog space). Regardless of the carefully observed fact that overall, tis particular model run indeed seems to over predict landslide volumes. To improve the model fit, there are three essential landslide parameters which will adjust landslide volumes : C, phi and t_{LS}. Calibrating those will be feasible following pathways outlined in section 4.3 of the manuscript. We agree with the reviewer that we could have stated this more clearly and will rephrase some of the sentences in the corresponding paragraph:

- Figure 8.b shows that HyLands is capable of approaching the shape of the universal Area-Volume relationships found by...
- While HyLands seems to overestimate simulated landslide volumes for very small landslides, the Area-Volume relationship simulated with HyLands approaches a linear relationship in a log-log space for larger landslides, similar to the shape of the observed Area-Volume relationship. Note that overall, landslide volumes simulated with HyLands are over predicted compared to observations. Study-area-specific model calibration would improve this fit but is beyond the scope of this model evaluation in which we evaluate the capacity of HyLands to reproduce the shape of the universal area-volume relationship. We attribute the positive deviation from the linear Area-Volume relationship in a log-log space for smaller landslides to the nature of the landslide algorithm: HyLands simulates deep-seated landslides, several of the smaller landslides are likely to be shallow landslides which are currently not simulated. Moreover, HyLands does not allow any sediment to be deposited within the landslide scar while this typically does occur in nature. Future developments of the algorithm could allow for shallow landsliding and in-scar deposition for more realistic simulations. ...

RC 1.3 — At what spatial scale is the drainage re-routing occurring? From Figure 9 (d, e, and f) and Figure 10, it does not seem that the channel profile's location has changed significantly. The figures make it seem like the channel moves on the order of one cell size due to valley blockage and the formation of epigenetic gorges. Could these slight reorganizations, over long periods, create major drainage reorganization or river piracy?

Reply: Again, a very insightful comment. Testing the impact of landslides on river capture and drainage reorganisation would be a natural avenue for follow up research activities. The model setup we used to showcase the impact of landslides on landscape evolution does however not provide the 'right' tectonic configuration to test this hypothesis. In our synthetic model run, we focus on the coupling between landslides and river-bed morphology. We therefore use a model set-up which is similar to the one used to evaluate the fluvial components of HyLands (Space). The initial surface of this run is a tilted plain which drains towards the southwestern corner, the only open boundary node. Therefore, from the first run steps onwards, all the water is forced toward this lower left corner. In order tho test whether the model actually reproduces river captures and drainage organisations, we suggest model setups with open flow boundary conditions. Moreover, you would probably like to test the impact of uplift or precipitation perturbations, which are, for the sake of simplicity and model demonstration, all kept constant in the current model runs.

RC 1.4 — Related, how computationally expensive is the landslide (non-linear deposition) routing compared to the rest of the model? I'm really excited for researchers to start using this model. I would be interested to know how fast the model runs, and how modifications that complicate or simplify the landsliding component of HyLands would affect the computational efficiency.

Reply: This is a relevant comment which we believe requires some attention given the aim of this paper (i.e. presenting a novel numerical model). The good news is that HyLands is fairly efficient both regarding landslide formation (the Culmann algorithm) as well as the sediment routing algorithm. In the updated version of the manuscript, we will added a row in the Table 1, indicating the average time required to complete one model iteration (Computation time per iteration). From the synthetic model runs, it can be seen that running HyLands with landslide erosion and sediment redistribution takes about double the time as it would when those processes are not simulated.

RC 1.5 — The first part of the model verification section details the steady-state behavior of detachment-limited, transport-limited, and mixed bedrock-alluvial landscapes. I would like authors to answer: How does the steady state behavior of a mixed bedrock-alluvial landscape with landslides as the sediment delivery mechanism compare to a simulation without landslides?. My guess would be that the main controlling parameter would be t_{LS}, the return time for landsliding. For very small values of t_{LS}, small frequent landslides will dominate; however, there will be little time for the landscape to recover/build up storage of landslide material. In this case, I believe the model would act very similarly to the initial runs in SPACE. For large t_{LS} values, large but seldom landslides dominate. If the landslides are very rare, I think the landscapes will also act similarly to SPACE. In between these two extremes, I think there is potential for the landscape to behave quite differently.

Reply: Evaluating the impact of landslides on long term landscape evolution is part of the motivation why we developed HyLands. Answering the question as to what extent landslides impact steady state landscape outlooks however opens up a bunch of other questions. A first question is related to the impact of different parameter values on the landslide erosion dynamics: the reviewer is right in his assessment that landslide return times t_{LS} will impact steady state landscape topography. However, equally important will be the cohesion factor C as well as the angle of internal friction ϕ. The way in which these factors influence landslide erosion patterns is currently not well understood. HyLands offers a tool to investigate these inter-dependencies using a suit of sensitivity analyses and by comparing simulated landslide patterns with observed landslide properties. Second, also the way in which landslide sediments are being distributed will influence 'steady state' landscape shapes. Again, running the model using a broad range of parameter values will improve our understanding as to what extend sediment redistribution influences landscape evolution. Parameters involved here are those controlling landslide sediment deposition on hillslopes after failure (Eq. 12, parameter Sc) as well as subsequent sediment redistribution by fluvial processes (the

SPACE parameters). Finally, the way in which landscapes evolve towards a steady state will be at least as important to evaluate as the steady state result of landscape evolution. Answers to all those questions are currently open for debate. Nevertheless, we believe that this manuscript is not the right place to answer them: we want to use this paper to present a novel model and to evaluate its basic functionality. Albeit showing the results of one particular model run where a landscape is evolving to steady state might answer some of the previous questions, the answer would be a partial one given the strong interdependency of all processes involved in HyLands. Understanding those interdependencies in a rigorous sensitivity analysis would be a first step in answering the question as to what extent landslides influence long term landscape dynamics. The reason we did run the model into a steady state without landslides (Fig. 5) is because we wanted to test if our model is capable to reproduce well established theoretical relationships on fluvial dynamics which currently do not exist for landslides. We believe however that the reviewer proposes a very interesting potential application of HyLands which we now address in the discussion section of the manuscript (under 4.4: Potential applications) where we added the following paragraph:
A particular question which remains open for debate is the way in which landslides influence the evolution of a landscape to steady state. Albeit the stochastic nature of landslides will prevent landscapes to evolve towards time and space invariant topographies, even with landslides, landscapes will evolve towards a quasi steady sate if external drivers such as climate and tectonics remain constant. Although our mechanistic understanding of landscapes strongly improved by studying steady state landscapes, an even more interesting and challenging question would be to study the impact of landslides on the dynamic evolution of a landscape towards such a steady state. The latter being more relevant for most real-world landscapes which are known to be rather in transient than a steady state (Mudd et al. 2017).

RC 1.6 — Please consider reading Zhang et al., 2018 (The Advective-Diffusive Morphodynamics of Mixed Bedrock-Alluvial Rivers Subjected to Spatiotemporally Varying Sediment Supply) paper which also considers the tool effect.

Reply: We thank the reviewer for pointing us to this paper. Shobe et al (2017) discussed similarities and differences between the SPACE model and the approach of Zhang et al (2015), which as we understand it is the same model used in Zhang et al (2018). We agree that the tools effect would be another interesting addition to the current model framework.

Minor

Reviewer Point 1.7 — Figure 2: Where is the function, $f(H/H\star)$, I do not think it is defined in the text. I am guessing it is $(1 - exp(\frac{-H}{H\star}))$ and $exp(\frac{-H}{H\star})$. Also, shouldn't the function be on the ordinate and the variable $H/H\star$ be on the absciss a?

Reply: The reviewer is correct about the form of the function $f(H/H\star)$. It is a good point that although these expressions occur in equations 3 and 4, $f(H/H\star)$ was never explicitly defined on its own. We have added its definition to the caption of Figure 2, and in the same place referenced the relevant governing equations (3 and 4).

Both reviewers commented on the choice of axes in this figure. We have reversed the ordinate and abcissa.

Reviewer Point 1.8 — Line 171: ”landslide” not “andslide”

Reply: Fixed.

Reviewer Point 1.9 — Line 252: citation for the sink filling algorithm?

Reply: Fixed.

Reviewer Point 1.10 — Figure 4: Not sure if this plot is made from actual data, but it would be interesting to show a similar figure before and after the landslide for visualization.

Reply: This is a hypothetical sketch. Adjusted the subscript by adding ’potentially initiate’

Reviewer Point 1.11 — Table 1: (a) after Synthetic should be a superscript?Also, you may want to draw another line in the table to make it clear that the Pre, LS-Event, and Post columns refer to the Synthetic landscape and not the Namche-Barwa.

Reply: Fixed.

Reviewer Point 1.12 — Table 2: Same as Table 1, it is not clear that Before intense LS period belongs to the Synthetic runs, instead of the Real DEM run.

Reply: Fixed.

Reviewer Point 1.13 — Line 349: Why did you choose 20,000 years for the return time?Would this value affect your results? If it is too long, perhaps you would not collect enough data to generate Figure 8.

Reply: Good question. We did not calibrate any of the model parameters for reasons discussed in the manuscript and in RP 1.2. Although the other parameters could be set to theoretical values, $t_L S$ is a new parameter introduced in this model. We therefore set the $t_L S$ to $2{\times}10^4$ years which is a rather arbitrary value. Parameter sensitivity runs in future work will show the impact of changing the landslide return times. We added the following sentence in the manuscript to clarify: Evaluation of model sensitivity to changing values for t_{LS} would be one of the natural avenues for further work.

Reviewer Point 1.14 — Figure 7: Should the unit be $m^{0.5}$, not m? Would log units be more useful?Also, perhaps switch the locations of E and D so D is on top, which corresponds to the color bar. Are the color bars for the 1st and 2nd column supposed to be different?Also, the figure caption shows the time steps for the 3rd column as 5, 500, 1500, and 2000 years, but the row titles show different values. Are they supposed to be different? Is so, why? Last, do landslides stop occurring in the simulation because of the absence of uplift?

Reply: All very good suggestions. Fixed to $m^{0.5}$. I definitely tried log units because those would be more familiar to the reader. Unfortunately, this does not really work out well since small erosion and deposition rates would end up being negative (values smaller than 1). This would prevent us from plotting erosion and deposition on the same plot. Color bars are the same, and since patterns of landslides are almost not different in the previous version of this figure, we dropped the colorbars.

There was an error in the caption. We removed this part of the caption as the years are already indicated in the first sentence of the caption. Landslides do not stop to occur. This is more clear on the new version of the figure. Given that the second reviewer also had some valuable suggestions for this figure, we made a new version of Figure 7.

Reviewer Point 1.15 — Figure 8b: I think there are missing symbols in the legend.

Reply: Sorry for that, we messed up the legend. The grey bar is now properly added to the figure.

Reviewer Point 1.16 — Figure 9 (also, Figure 10 and movies): I think the color bar for topography in panels (a), (b), and (c) are incorrect. It should be from 0 to 300 meters, not 0 to 1meter.

Reply: You are absolutely right. We corrected this in both the figures and the movies. Moreover, we made several additional adjustments to this figure in order to improve clarity and to get the message better across (see also SP 2.36)

Reviewer Point 1.17 — Figure 9 caption: I think there should be more explanation of how epigenetic gorges are formed in the text. I believe the river jumps out of its original channel after being filled by alluvium and is routed on bedrock. How sensitive is this behavior to the algorithm used to fill sinks?

Reply: We rephrased the corresponding paragraph in the text as:
The drainage re-routing mechanism dominates in the simulations presented here and results in the formation of epigenetic river gorges (Fig. 9). Epigenetic river gorges are characterized by rivers incising into the bedrock of former valley walls due to the blockage of the formal channel by landslide derived sediment (Ouimet et al. 2008).
Regarding the sensitivity to the fill algorithm: after landslide blockage of the river path, a fill algorithm is used to identify landslide lakes and water is rerouted following the steepest path using a D8 flow direction algorithm.

Reviewer Point 1.18 — Figure 10: Where is the rerouting? The channel pathway looks the same to me; is there a better way to illustrate the rerouting?

Reply: The rerouting happens on Figure 9, when landsliding kicks in. A major rerouting happens right after the start of the LS simulations (Fig 9.c to the LS Fig.9, d). Small changes to the flow path continue to occur from Fig. 9.d to f. Once landsliding stops, the channels are not blocked any longer and will mostly stay in place (Fig. 10)

Reviewer Point 1.19 — Line 417: Can you show knickpoint generation with a distance upstream vs.slope plot? The knickpoints are very apparent in the movies, but I do not think a series of topographic profiles would show the knickpoint adequately.

Reply: We do not fully understand this comment. We believe the presence of knickpoints is very apparent on Fig. 9 d-f. We added a reference to this figure in the manuscript to enhance clarity. We also added some text to better explain the phenomena of epigenetic river gorges.

Reviewer Point 1.20 — Line 419: "Figs." not "Fig. s"

Reply: Thanks. Fixed.

Reviewer Point 1.21 — Line 453: Please consider citing Zhang et al., 2018.This paper looks at how varying sediment transport inputs (e.g. from landsliding) affects bedrock erosion with a tools and cover model.

Reply: Done, see also comment before.

Reviewer Point 1.22 — Line 528: I would be very interested if your model can reproduce this.

Reply: We too.

Reviewer 2

Alexander Densmore

Summary: This is a very well-written manuscript that makes a clear contribution to knowledge.The authors have combined an elegant new fluvial landscape evolution model with an existing approach to modelling bedrock landslides. The result is, to my knowledge, the only modern landscape evolution model that explicitly accounts for bedrock landslides,and that will therefore allow a number of new problems to be addressed. The authors have done a very good job of summarising both the model and some of these potential applications. I have made some comments and suggestions on the manuscript PDF, which I will paper not repeat here. Most of these are minor and relate to clarification of a few points or requests for a little more information. These should be straightforward for the authors to address. The only more substantive questions relate mostly to the figures,especially Figs 7-10. The text and captions don't fully explain what these figures are showing, making it hard for the reader to fully understand the results. The text describes changes in the lateral position of the river system due to landsliding, but I really don't think that Figs 9-10 show this clearly or effectively. As this seems to be one of their main take-home messages about the impact of landsliding on these landscapes, I think that they could perhaps do more to show these changes to the reader. Once these relatively minor issues are addressed, however, then the revised manuscript should be ready for publication.

Reply: We explicitly want to thank the reviewer, Alexander Densmore, to review our manuscript in such a short period, given the challenging times. We are pleased that the reviewer appreciates our work. Minor comments regarding typos and text edits are addressed directly in the updated version of the manuscript.

Reviewer Point 2.1 — Line 6 - remove earth

Reply: Fixed.

Reviewer Point 2.2 — Line 64 - This isn't actually the case - I had to go back and check! We used the lowest point on a hillslope that fit the failure criteria, but that point did not need to be in the channel. As stated on p. 15,208, 'This ensures that landslides begin near the toes of hillslopes', but not necessarily at the toe. Line 66 - As above, this isn't what was done in that paper, so I suggest cutting this. You're absolutely right that sediment is spread at a constant slope and that there's absolutely nothing mechanistic about the approach, however.

Reply: Thanks for clarifying this and apologies for misinterpreting this. We removed this sentence and rephrased to: (i) all hillslopes behave as Mohr-Coulomb materials (Taylor et al. 1948), (ii) landslides initialize near the toes of hillslopes and (iii) landslide-derived sediment is spread under a constant slope, following the steepest downslope path.

Reviewer Point 2.3 — LLine 76 - The wording here is a little confusing - it sounds like the processes aren't available at large scales, which isn't what you mean. I suggest rewording as something like '...processes, and require input parameters which may not be adequately known at large spatial scales.'

Reply: Good suggestion, we rephrased accordingly.

Reviewer Point 2.4 — Line 81 - While the text above is very clear on what has been done to date, I feel like there is a sentence missing that just puts those pieces together into a single statement that motivates your work. In other words: what's the specific gap that you will now be able to fill?

Reply: We added the following sentence: Notwithstanding the prominent role of landslides in shaping the earth surface and controlling sediment supply and transport, few efforts have been made to actively simulate the impact of stochastic landsliding on landscape evolution and sediment dynamics over large spatial and temporal scales.

Reviewer Point 2.5 — Line 107 - due to landsliding

Reply: Fixed.

Reviewer Point 2.6 — Line 112 - This was already defined on line 58

Reply: Fixed.

Reviewer Point 2.7 — Line 116 - OK... with the caveat that this is also going to depend upon the spatial resolution of the model and the way in which rivers are modelled in the grid - i.e., whether or not they are treated as a single thread of cells, or whether the equations are applied to the whole landscape. I presume it's the latter although this isn't explicitly stated

Reply: We added two sentences to the previous paragraph for clarification: Note that HyLands does not explicitly distinguish between river or hillslope cells: all equations are applied to the entire landscape. Processes affecting sediment thickness and bedrock elevation in each cell can be either fluvial dynamics (SPACE), landslides, or a combination of both, hence the hybrid nature of HyLands. Moreover, as suggested by A. Densmore, we moved the following sentence from the discussion to this point in the manuscript: Note that this approach implies that all river cells in the landscape are assumed to occupy 1 grid cell with distance dx, that channel width may be less than, equal to, or greater than dx, and that river width is only a function of contributing drainage area.

Reviewer Point 2.8 — Line 135 - the

Reply: Fixed.

Reviewer Point 2.9 — Line 155 - Can you remind us (briefly) how this is determined?

Reply: We added the following sentences to clarify: V is the net effective settling velocity, which represents the still-water particle settling velocity corrected for the upward effects of turbulence and the vertical gradient in sediment concentration through the water column (Davy and Lague, 2009). HyLands enables spatially variable values for V to distinguish between settling velocities over flooded versus non-flooded nodes.

Reviewer Point 2.10 — Figure 2: There is a slight mismatch with the text here, given that the text doesn't refer to f at all, but simply builds negative exponential functions of H/H* into eqns 3 and 4. I wonder, therefore, if it's more straightforward to flip this by 90 deg and to relate this more clearly to eqns 3 and 4. I get the echoes here of the tools/cover effect plots, but I think it's potentially a bit confusing as currently designed. Just a thought.

Reply: Good point. We flipped the axes as suggested, and defined $f\,(H/H_*)$ in the figure caption. We also referenced the relevant erosion/entrainment equations in the caption to make the function notation less confusing.

Reviewer Point 2.11 — Line 207 - plane

Reply: Fixed.

Reviewer Point 2.12 — Line 208 You use both node and pixel in this section - are they equivalent? If so then I suggest using one term or the other; if not then please explain the distinction.

Reply: Good point. We use the term 'cell' now throughout the text

Reviewer Point 2.13 — Line 217 - Suspended sediment makes sense here - I'm struggling to envision a situation, however, where a measurable volumetric fraction of hillslope sediment contributes instantly to the dissolved load of the river. Perhaps cut, unless I'm missing something?

Reply: We dropped dissolved

Reviewer Point 2.14 — Line 222 - True - and also doesn't account for different depositional slopes for different landslide bulk rheologies or grain size distributions...

Reply: Thanks for clarifying

Reviewer Point 2.15 — Line 230 - an approach

Reply: Fixed.

Reviewer Point 2.16 — Line 232 - landslide-derived

Reply: Fixed.

Reviewer Point 2.17 — Line 245 - ... and there is no deposition at that cell?

Reply: We added these words for clarification.

Reviewer Point 2.18 — Line 246 - Is this the angle of the surface of the resulting deposit? If so, then maybe call it a minimal deposit surface angle. 'Spreading angle' could be confused with spreading across multiple flow directions.

Reply: Good suggestion. We adjusted the text accordingly throughout the manuscript

Reviewer Point 2.19 — Line 249 – Should this be changed to 'over the landscape'? Presumably the spreading algorithm distributes sediment downslope, whether or not the target cell is a hillslope or channel cell. This comes back to an earlier question - is there any distinction made between hillslope and channel cells, or are the model equations applied to the whole landscape? The previous text suggests the latter, but this sentence might imply that there is a difference. It would be great if you could clarify this.

Reply: Good that you point us to this. We added a couple of sentences right after the GMB equation (Eq. 5) to clarify. See also reply to earlier comment (2.7)

Reviewer Point 2.20 — cfr. == cf. ?

Reply: Fixed

Reviewer Point 2.21 — Line 251 - Again - are nodes and cells the same thing? If so then it would be good to use a consistent term.

Reply: Good point. We use the term 'cell' now throughout the text

Reviewer Point 2.22 — Line - 272 conditions?

Reply: Fixed

Reviewer Point 2.23 — Table 1 - It took me awhile to realise that (a) referred to a note at the bottom of the table - perhaps make this superscript to match the others?

Reply: Fixed

Reviewer Point 2.24 — Table 1 - I suggest inserting a space (m yr^{-1}), to avoid confusion.

Reply: Fixed

Reviewer Point 2.25 — Table 1 - This should be mentioned explicitly in section 2, rather than defined in the table notes

Reply: We added this information in the main text of the manuscript, after introducing Eq. 5, see also reply to earlier comment (2.9)

Reviewer Point 2.26 — Line 310 - Applying HyLands to the Namche Barwa-Gyala Peri massif I don't have any issue with this application... but I find it a slightly odd choice, not least because of the very limited field data available to ground-truth the Larsen and Montgomery landslide inventory. Given the rapidly-growing number of well-constrained inventories out there, why did you choose this particular one? The pre-1974 inventory is particularly poorly constrained in terms of the time scale that it covers, and both inventories suffer from extreme orthorectification issues caused by the steep topography. There's also nothing known about the history of either rainfall or earthquake landslide triggers in that area, other than the big 1950 event which almost certainly triggered some of the events in the inventory. It's not a bad choice to evaluate the model, but it just seems like there are other inventories out there that fit your requirements better. I'd be curious to see an additional line in the text that gives the reason why this was chosen.

Reply: Again, a very insightful comment. We agree with the reviewer that if the aim of this exercise would be to exactly reconstruct an observed LS inventory, other regions would probably make up for a better application for reasons given by the reviewer. However, our intention is not to calibrate HyLands to a specific study area, neither to reproduce exact magnitude frequency distributions because these would indeed require detailed information on earthquake and storm histories. Rather we were interested if we could reproduce the general shape of the empirical and universally observed magnitude frequency and area-volume relationships. The question remains as to why we selected the Namche Barwa-Gyala Peri massif as an area to test HyLands. We now address this issue in the manuscript by adding the following lines of text:
We selected the Namche Barwa-Gyala Peri massif to evaluate the performance of HyLands given its unique geomorphologic configuration featuring amongst the highest globally documented river stream power in combination with very active hillslope processes (Larsen, 2012). With HyLands being designed to couple the role of fluvial and hillslope processes, this region makes up for a good test environment. Note however that we do not intent to calibrate neither validate the model but run it using fixed, theoretical model parameters (section 3.2.3). Applications of HyLands aiming to constrain the model through parameter calibration and validation (section 4.3) would require additional data to ground-truth landslide inventories and to provide detailed records on landslide triggers such as earthquakes and storms.
Also note the reply to Reviewer 1, which is related to this comment (see RC 1.2)

Reviewer Point 2.27 — Line 320 - Out of curiosity, why would you do this?

Reply: We address this question in the manuscript now: We resampled the DEM to a resolution of 20 m in order to evaluate the capacity of HyLands to reproduce the rollover in the magnitude frequency distribution, often reported to occur for landslide areas < 900 m^2, which would be the minimum landslide area when using the original SRTM data.

Reviewer Point 2.28 — Line 342 - It's not clear what this text is doing within the citation - perhaps rework this into the sentence.

Reply: Fixed

Reviewer Point 2.29 — Figure 7 - It's quite hard to see the detail in this figure without zooming way in - I wonder if you can make more efficient use of the space by increasing the size of the panels. Given that the colorbars for each row are almost identical, do they need to be shown 4 times?

Reply: Good suggestion, we remade the figure.

Reviewer Point 2.30 — Figure 7 - I might be missing something, but the left-hand column just seems to show landslide locations - I can't see anything that follows the red-to-blue color scale indicated. The other two colorbars seem to fit with the middle and right-hand columns, but what are the colors meant to indicate on the left-hand column?

Reply: Good point. Actually in the left hand column of the previous figure, you can see the landslides if you would zoom in closely. However, as this is very difficult to see, we removed the colorbar for these figures.

Reviewer Point 2.31 — Figure 7 - It's not very clear what you're plotting. All of your model parameters relating to erosion and deposition are represented as rates, with units of L/T. So it's not obvious why you've taken the square root of those quantities and how you've kept units of meters. I understand that this won't affect the patterns that you show, but I think this could be more clear to the reader.

Reply: This remark is similar to the one made by reviewer 1. We corrected the units to $\sqrt{m}$. See also SP 1.14

Reviewer Point 2.32 — Figure 7 - Rather than referring to this as 'SED' in the figure, it would be better to relate this back to the parameters that you have already defined and used throughout the manuscript so far. Is this the same as H in equation 1?

Reply: Yes, this is H, we changed the label of the colorbar.

Reviewer Point 2.33 — Line - 360 I'm not sure where that can be seen on Fig 7 - perhaps point it out?

Reply: Good suggestion. We now point it out explicitly: e.g., the deposition pattern in Fig. 7.h reflects the shape of erosion patterns resulting from previous landslide activity

Reviewer Point 2.34 — Figure 8 - Rather than 'PDF', it might be better to label this for what it is, which is the spatial frequency density of landsliding per unit area

Reply: Good suggestion, we will adjust

Reviewer Point 2.35 — Figure 8 - This may be a problem with the PDF conversion, but the symbol for this zone seems to be missing from the legend on the figure, along with the best-fit regression line

Reply: Sorry for that. We messed up the legend of the figure, this is fixed now

Reviewer Point 2.36 — Figure 9 - The caption for this figure is a little bit lacking, in that it's not clear what is being plotted. What's the difference between the top-left and top-right subfigure in each panel? What does the blue line in each panel represent? Why is the brown line labelled 'Current Topo' in the left-hand column, but seems to correspond to 'Sediment' on the right-hand y-axis? The brown lines seem to show different things in the two columns, so I'd suggest making these distinct. Also, confusingly, blue areas seem to denote sediment on the profiles in the left-hand column, but water in the profiles on the right - I didn't realise that this was the case until I got to Fig. 10 a couple of pages later. This is a really interesting figure - a little more care with the colors, labels, and caption would really help the reader to get the most out of it.

Reply: Thanks a lot for these very useful recommendations. We adjusted the labels on the figure and changed the figure caption as follows: **(a-d)** Time slices showing evolution of the landscape to steady state, before the landslide period. The upper left subplots show the evolution of topography through time. The upper right subplots show the evolution of of sediment thickness (H) through time. On both subplots, the blue line represents the location of the river, plotted in the lower subplots. These lower subplots show the topographic and bedrock elevation (red and black line respectively). The difference between the topographic elevation and the elevation of the bedrock represents the sediment thickness. With respect to total elevation, sediment thickness is small, which is why sediment thickness (orange line) is also plotted against a separate right-hand y-axis. The gray shaded area represents bedrock underlying the river profile. **(e-h)** Time slices showing the landslide period where intense landsliding is occurring over a period of 100 years. The upper left subplots show the landslide activity. The location of landslides is indicated with black diamonds. The colors represent the square root of the landslide erosion (-) and deposition (+) during the presented time step. The upper right subplots show the evolution of of sediment thickness (H) through time. On both subplots, the blue line represents the location of the river, plotted in the lower subplots. These lower subplots show the topographic and bedrock elevation (red and black line respectively) as well as the volume occupied by sediments and water (orange and blue shaded area respectively). Note that, during landsliding, both pure landslide dams arise as well as irregularities in the bedrock profile (the grey bumps). The latter originate from the river being redirected after landsliding forming epigenetic gorges (see text). We adjusted Figure 10 accordingly.

Reviewer Point 2.37 — Line 402 - I don't understand - does this mean that the profile is always taken in the same place, but that in some places that profile corresponds to the active channel and in other places it doesn't (when the channel has been diverted to a different location)? Or are those bumps areas where bedrock incision and lowering of the channel bed has been inhibited by the addition of large volumes of sediment?

Reply: We agree that this was a confusing sentence and removed it from the manuscript. Instead, we now elaborate on this issue in the next paragraph by extending our explanation on the formation of epigenitic gorges. This comment is similar to the remark of reviewer 1, addressed in RC 1.3 and one of the following remarks (PT 2.39)

Reviewer Point 2.38 — Line 407 - Just to clarify, landslide sediment has the same transport coefficient as any other sediment in the model, right? So there is no 'immobile debris'?

Reply: Correct, we removed immobile

Reviewer Point 2.39 — Line 412 - I'm not sure that I would call that 'drainage re-routing', as that implies a lateral shift in the position of the active channel. Is that what you mean?

Reply: We actually mean to describe such a lateral shift. We rephrased the corresponding paragraph in the text as:
The drainage re-routing mechanism dominates in the simulations presented here and results in the formation of epigenetic river gorges (Fig. 10). Epigenetic river gorges are characterized by rivers incising into the bedrock of former valley walls due to the blockage of the formal channel by landslide derived sediment (Ouimet et al. 2008).

Reviewer Point 2.40 — Line 457 - See my earlier queries on section 2 - this information could usefully be included there.

Reply: Good suggestion, we move this sentence to section 2. See also reply SP 2.7 .

Reviewer Point 2.41 — Line 494 - True... or even with medium-complexity approaches such as RAMMS or Flow-R...

Reply: Indeed, we added those and corresponding references

Reviewer Point 2.42 — Line 509 - True. You could cite Fan et al. (2018) Landslides as an example where this has been done, or Fan et al. (2019) Rev of Geophys as a good review of the problem.

Reply: Absolutely, a reference to the review of Fan et al. was intended here, good that you point us this

Reviewer Point 2.43 — Line 519 - them: Not sure what you're referring to here.

Reply: We adjusted the sentence

Reviewer Point 2.44 — Line 526 - OK - so, given the results of those studies, as well as the recent work by Thomas Croissant as well as some of the authors, what are the most pressing remaining questions or issues?

Reply: One example of a pressing remaining question has been suggested by reviewer 1 and is now added as a potential application to this paragraph (see also RC 1.5): A particular question which remains open for debate is the way in which landslides influence the evolution of a landscape to steady state. Albeit the stochastic nature of landslides will prevent landscapes to evolve towards time and space invariant topographies, even with landslides, landscapes will evolve towards a quasi steady sate if external drivers such as climate and tectonics remain constant. Although our mechanistic understanding of landscapes strongly improved by studying steady state landscapes, an even more interesting and challenging question would be to study the impact of landslides on the dynamic evolution of a landscape towards such a steady state. The latter being more relevant for most real-world landscapes which are known to be rather in transient than a steady state (Mudd et al. 2017).

Reviewer Point 2.45 — Line 530 - ... or to a major landslide triggering event. See, for example, some of the work after the 2015 Gorkha earthquake that speculated on this exact point.

Reply: Good suggestion. We rephrased and inserted some additional references as: Second, HyLands can be used to evaluate the response time of a landscape to a major landslide triggering event and to understand the timescales over which landslide-derived sediments are exported from the landscape (Wang et al., 2015; Li et al.,2016; Schwanghart et al., 2016; Robinson et al., 2017; Roback et al., 2018)

HyLands 1.0: a Hybrid Landscape evolution model to simulate the impact of landslides and landslide-derived sediment on landscape evolution

Benjamin Campforts[1,2], Charles M. Shobe[1], Philippe Steer[3], Matthias Vanmaercke[4], Dimitri Lague[3], and Jean Braun[1,5]

[1]Helmholtz Centre Potsdam, GFZ German Research Centre for Geosciences, Potsdam, Germany
[2]Institute for Arctic and Alpine Research, University of Colorado at Boulder, Boulder, CO, USA
[3]Univ Rennes, CNRS, Géosciences Rennes – UMR 6118, 35000 Rennes, France
[4]Université de Liège, UR SPHERES, Département de Géographie, Clos Mercator 3, 4000 Liège, Belgium
[5]Institute of Earth and Environmental Science, Universität Potsdam, Potsdam, Germany

Correspondence: Benjamin Campforts (benjamin.campforts@gfz-potsdam.de)

Abstract. Landslides are the main source of sediment in most mountain ranges. Rivers then act as conveyor belts, evacuating landslide-derived sediment. Sediment dynamics are known to influence landscape evolution through interactions among landslide sediment delivery, fluvial transport, and river incision into bedrock. Sediment delivery and its interaction with river incision therefore control the pace of landscape evolution and mediate relationships among tectonics, climate, and erosion. Numerical landscape evolution models (LEMs) are well suited to study the ~~interaction among these earth~~ interactions among these surface processes. They enable evaluation of a range of hypotheses at varying temporal and spatial scales. While many models have been used to study the dynamic interplay between tectonics, erosion and climate, the role of interactions between landslide-derived sediment and river incision has received much less attention. Here, we present HyLands, a hybrid landscape evolution model integrated within the Topo Toolbox Landscape Evolution Model (TTLEM) framework. The hybrid nature of the model lies in its capacity to simulate both erosion and deposition at any place in the landscape due to fluvial bedrock incision, sediment transport and rapid, stochastic mass wasting through landsliding. Fluvial sediment transport and bedrock incision are calculated using the recently developed Stream Power with Alluvium Conservation and Entrainment (SPACE) model. Therefore, rivers in HyLands can dynamically transition from detachment-limited to transport-limited, and from bedrock to bedrock-alluvial to fully alluviated states. Erosion and sediment production by landsliding ~~is~~ are calculated using a Mohr-Coulomb stability analysis while landslide-derived sediment is routed and deposited using a multiple flow direction, non-linear deposition method. We describe and evaluate the HyLands 1.0 model using analytical solutions and observations. We first illustrate the functionality of HyLands to capture river dynamics ranging from detachment-limited to transport-limited ~~configurations~~conditions. Second, we apply the model to a portion of the Namche-Barwa massif in Eastern Tibet and compare simulated and observed landslide magnitude-frequency and area-volume scaling relationships. Finally, we illustrate the relevance of explicitly simulating landsliding and sediment dynamics over longer timescales for landscape evolution in general

and river dynamics in particular. With HyLands we provide a new tool to understand both the long and short-term coupling between stochastic hillslope processes, river incision, and source-to-sink sediment dynamics.

1 Introduction

Landsliding is a highly effective erosional mechanism that dominates sediment mobilization rates in moderate to steep topographic settings (Hovius et al., 1997; Ouimet et al., 2007; Broeckx et al., 2020). Nonetheless, long term landscape evolution in non-glaciated settings is mainly controlled by the interplay between tectonic uplift and fluvial dynamics (Whipple and Tucker, 1999; Wobus et al., 2006). Fluvial channels in mountainous catchments play a dual role: they simultaneously incise into the bedrock and act as conveyor belts to carry eroded sediment out of the mountain range towards the ocean (Milliman and Meade, 1983). Through sediment evacuation and bedrock incision, fluvial incision lowers the base level for surrounding hillslopes, triggering hillslope failures. In turn, hillslope failure through mass wasting chokes the rivers with sediment and prevents further bedrock incision until ~~landslide derived~~ landslide-derived sediment has been evacuated from the system (Larsen and Montgomery, 2012; Ouimet et al., 2007; Korup et al., 2010; Shobe et al., 2016; Glade et al., 2019).

Unravelling the dynamic interplay between landslides and fluvial processes is key to understanding long-term landscape evolution and the associated sediment dynamics in mountainous terrain (Egholm et al., 2013). Increased insight into the spatial distribution of landslides has resulted in improved landslide susceptibility assessments (Guzzetti et al., 2006), but processes regulating landslide rate assessments (Broeckx et al., 2020) and landslide-derived sediment dynamics remain less well understood (Hovius et al., 2011; Croissant et al., 2017, 2019; Zhang et al., 2019; Broeckx et al., 2020).

Numerical models are excellent tools to study relationships between processes regulating Earth surface dynamics and their inter-dependencies over various temporal and spatial scales (Tucker and Hancock, 2010). The past twenty years have seen the development of a plethora of Landscape Evolution Models (LEMs), enabling studies of the interactions among climate, tectonics, and erosion. A crucial ingredient for any LEM is a fluvial erosion component regulating the way in which rivers transport sediment and incise into bedrock. Fluvial incision is controlled by both water and sediment cascading through river channels (Whipple et al., 2000; Hancock and Anderson, 2002; Turowski et al., 2007). Most existing LEMs simulate river incision using one of two commonly used ~~end member models to simulate fluvial dynamics~~ end-member models (Armitage et al., 2018). In one approach, river incision is simulated assuming a detachment-limited configuration where erosion is constrained by the power to erode particles from the river bed and quantified using a scaling law between fluid stress and river incision rate (Seidl and Dietrich, 1992; Howard and Kerby, 1983; Campforts and Govers, 2015). In the other approach, river incision is simulated assuming a transport-limited configuration where erosion is constrained by the capacity of the river to carry sediment, where the carrying capacity is a function of the fluid stress (Willgoose et al., 1991; Paola and Voller, 2005). These two formulations lead to similar outcomes in steady-state channels (where the river erosion rate equals the rock uplift rate), but noticeably different outcomes during transient river response to tectonic and climatic perturbations (Whipple and Tucker, 1999).

In real settings, however, even steep mountain channels undergoing long-term bedrock incision may experience bed cover by alluvial sediment. Further, over geologic time as tectonic and climatic forcings change, it is likely that any given channel transitions between detachment-limited and transport-limited behavior. Such heterogeneous configurations require a model setup that can dynamically transition between detachment-limited and transport-limited regimes (e.g., Davy and Lague, 2009) and can simultaneously simulate fluvial sediment transport and river incision into bedrock (e.g., Lague, 2010). Recently, the SPACE (Stream Power with Alluvium Conservation and Entrainment) model approach was proposed to meet both of these needs (Shobe et al., 2017). Because SPACE is purely a river incision model, it does not simulate hillslope or mass wasting processes. Additional model components are therefore needed to simulate the impact of mass wasting on landscape evolution and sediment dynamics.

To understand how landslides influence landscape evolution, Densmore et al. (1998) proposed an approach, adapted by others (e.g. Champel, 2002; Egholm et al., 2013), to integrate stochastic landslide dynamics in a numerical landscape evolution model. Densmore et al. (1998) assume that (i) all hillslopes behave as Mohr-Coulomb materials (Taylor, 1948), (ii) landslides initialize in river channels (i.e. at the base of hillslopes) near the toes of hillslopes and (iii) landslide-derived sediment is spread under a constant slope, following the steepest downslope path. Assuming that landslides initialize only in fluvial channels makes it computationally easier to implement a landslide model because sediment pathways on hillslopes need not be calculated. However, it is not realistic to neglect landslides that might initiate away from river channels: it has been shown that a large portion of landslide-derived sediment is stored along flow paths on hillslopes, rather than being immediately delivered to river channels (Broeckx et al., 2020; ?). The approach of Densmore et al. (1998) does not allow for landslide-derived sediment to be deposited and spread over hillslopes. Rather, landslide debris is spread as tongues of sediment filling up the river channel.

Other researchers have developed mechanistic models to simulate shallow landslide activity at the landscape scale (e.g. Montgomery and Dietrich, 1994; Claessens et al., 2007). Such models typically involve the explicit simulation of a soil layer and a coupled hydrologic model to calculate how changing pore water pressures trigger landslides (Van Asch et al., 1999; Iverson, 2000; Baum et al., 2010). Although such mechanistic models are useful for assessing landslide hazards (e.g. to simulate landslide liquef (e.g. to simulate landslide liquefaction associated with the Oso landslide, cf. Iverson and George, 2016), they typically involve a range of geophysical processesand associated , and require input parameters which are not always available may not be adequately known at large spatial scales. This can make the more detailed models sensitive to equifinality (Beven and Freer, 2001). Moreover, deep-seated bedrock landslides, rather than shallow landslides, mobilize the largest volumes of sediment and therefore have the largest impact on landscape evolution (Burbank, 2002; Dussauge et al., 2003; Jeandet et al., 2019; Korup et al., 2007; Broeckx et al., 2020).

Notwithstanding the prominent role of landslides in shaping Earth's surface and controlling sediment supply and transport, few efforts have been made to actively simulate the impact of stochastic landsliding on landscape evolution and sediment dynamics over large spatial and temporal scales. In this paper, we present HyLands, a new Hybrid Landscape evolution model for simulating the interaction of landslide dynamics and fluvial processes. The model is intended to simulate Earth surface evolution at large spatial scales with a special focus on landsliding and the long-term effects of landslide-derived sediment. HyLands is integrated in the TTLEM 1.0 landscape evolution model (Campforts et al., 2017). Unlike the existing implementation of TTLEM, HyLands is a fully mass conservative model where fluvial dynamics are modelled using the SPACE fluvial incision framework (Shobe et al., 2017) and hillslope-derived sediment fluxes are explicitly simulated. In this paper, we first describe the fluvial and landslide components of the HyLands model. We verify the fluvial model component by comparing model behavior against known analytical solutions. Subsequently, we evaluate the performance of the landslide module by applying HyLands to a selected region of the landslide-prone Namche-Barwa massif in Eastern Tibet. We show that HyLands reproduces observed landslide scaling relationships. Next, we apply the model to a synthetic case to illustrate the potential of HyLands for studying the dynamic interaction between landslide activity and fluvial dynamics. We do this by evaluating how a steady-state landscape responds to an imposed pulse of landsliding activity. Finally, we discuss the current model limitations, future perspectives and a range of potential applications.

2 HyLands model description

HyLands is a Matlab model code building on the existing TopoToolbox Landscape Evolution Model (TTLEM, Campforts et al., 2017). It simulates changes in bedrock height and sediment thickness on a regular grid. The model is mass conservative; sediment produced by river incision and hillslope processes such as landsliding is explicitly simulated in the model. At every model iteration, the elevation of all grid cells is updated according to the following conservation statement for sediment and rock:

$$\begin{aligned}\frac{\partial \eta}{\partial t} =& \frac{\partial R}{\partial t} + \frac{\partial H}{\partial t} \\ =& U - E_{r_{fluv}} + \left(\frac{D_{s_{fluv}} - E_{s_{fluv}}}{1-\phi_{sed}}\right) \\ & - E_{r_{hill}} + \left(\frac{D_{s_{hill}} - E_{s_{hill}}}{1-\phi_{sed}}\right)\end{aligned} \quad (1)$$

where η $[L]$ is the topographic elevation given by the sum of the bedrock elevation R $[L]$ and the bed sediment thickness H $[L]$. U $[L/T]$ is the rock uplift rate and ϕ_{sed} is the bed sediment porosity. $E_{r_{fluv}}$ $[L/T]$ is the fluvial volumetric erosion flux of bedrock per unit bed area, representing the amount of bedrock that is detached and entrained into the water column. $E_{s_{fluv}}$ $[L/T]$ is the fluvial volumetric entrainment flux of sediment per unit bed area and $D_{s_{fluv}}$ $[L/T]$ is the fluvial volumetric deposition flux of sediment per unit bed area. $E_{r_{hill}}$ $[L/T]$ is the volumetric flux of hillslope bedrock erosion (landslding) due to landslding per unit bed area, representing the amount of bedrock that is detached. $E_{s_{hill}}$ $[L/T]$ is the volumetric entrainment flux of sediment erosion (produced by landsliding or creep) per unit bed area and $D_{s_{hill}}$ $[L/T]$ is the volumetric deposition flux of hillslope-derived sediment per unit bed area.

2.1 ~~River sediment transport and bedrock erosion~~

~~HyLands uses the Stream Power with Alluvium Conservation and Entrainment~~ Note that HyLands does not explicitly distinguish between river or hillslope cells: all equations are applied to the entire landscape. Processes affecting sediment thickness and bedrock elevation in each cell can be either fluvial dynamics (SPACE), landslides, or a combination of both, hence the hybrid nature of HyLands.

2.1 River sediment transport and bedrock erosion

HyLands uses the SPACE river erosion model of Shobe et al. (2017). SPACE has two key advantages for the purposes of modeling river response to landslide sediment delivery. First, because of its derivation from the erosion-deposition family of models (e.g., Beaumont et al., 1992; Davy and Lague, 2009), it can dynamically shift between detachment-limited (erosion is limited by the rate of sediment or bedrock detachment from the bed) and transport-limited (erosion is limited by the capacity of the flow to move detached sediment) behavior. Second, it can simulate the full continuum of possible river bed compositions from bare bedrock channels to mixed bedrock-alluvial channels to fully alluvial channels. This is accomplished by combining mass conservation of river bed sediment with a bedrock erosion law to simultaneously solve for the time evolution of the bedrock and sediment surfaces. Note that this approach implies that all river cells in the landscape are assumed to occupy 1 grid cell of width dx, that channel width may be less than, equal to, or greater than dx, and that river width is only a function of contributing drainage area. We implement the SPACE model equations in the TTLEM MATLAB modeling framework. For a full overview of the SPACE model and comparison with other models for coupled sediment and bedrock channel evolution, see Shobe et al. (2017).

2.1.1 Fluvial sediment and rock mass conservation

Conservation of sediment closely follows the erosion-deposition approach of Davy and Lague (2009), with the addition of terms that represent the entrainment of detached bedrock in the water column (Fig. 1). The spatial change in volumetric sediment flux Q_{sfluv} $\left[L^3/T\right]$ per unit width w $[L]$ is written as:

$$\frac{\partial \left(Q_{sfluv}/w\right)}{\partial x} = E_{s_{fluv}} + \left(1 - F_{f_{fluv}}\right) E_{r_{fluv}} - D_{s_{fluv}}. \tag{2}$$

where $F_{f_{fluv}}$ is a unitless fraction of fine fluvial sediment. The factor $1 - F_{f_{fluv}}$ $[-]$ represents the idea that a fraction of the bedrock particles detached from the bed may be small enough to stay in permanent suspension, and therefore should not be tracked as bed sediment.

2.1.2 Fluvial sediment entrainment, bedrock erosion, and sediment deposition

To evaluate the impact of landslide-derived sediment on landscape evolution, it is critical to have a model that simulates simultaneous sediment entrainment and bedrock erosion, and considers the influence of sediment cover on river erosion dynamics. In the SPACE model, sediment entrainment and bedrock erosion may occur simultaneously. Further, the magnitude of each process is set by the relative availability of sediment on the channel bed. SPACE accomplishes this by including the influence of the sediment layer on sediment and bedrock erosion rates.

Sediment entrainment and bedrock erosion are both governed by a unit stream power expression in which erosive power is a function of water discharge per unit width q $\left[L^2T^{-1}\right]$ and local channel slope S (e.g., Howard and Kerby, 1983; Whipple and Tucker, 1999; Davy and Lague, 2009). The sediment ~~erosion~~ entrainment rate $E_{s_{fluv}}$ and the bedrock erosion rate $E_{r_{fluv}}$ are modified by a term H/H_* $[-]$ that encapsulates the ratio of bed sediment thickness H $[L]$ to bedrock bed roughness H_* $[L]$. High bed sediment thickness or low bedrock surface roughness leads to a condition in which H/H_* is large and little bedrock is exposed to erosive flows. If bed sediment thickness is low or bedrock roughness is high, H/H_* is small and most of the in-channel bedrock is exposed to the flow.

SPACE assumes an exponential increase in sediment entrainment rate with increasing H/H_* and a concomitant exponential decrease in bedrock erosion rate with increasing H/H_* (Fig. 2). Rates of sediment entrainment and bedrock erosion can therefore be written as (assuming a negligible erosion threshold; see Shobe et al. (2017) for equations that relax this assumption):

$$E_{s_{fluv}} = K_s q S^n \left(1 - e^{-H/H_*}\right) \tag{3}$$

for sediment and

$$E_{r_{fluv}} = K_r q S^n e^{-H/H_*} \tag{4}$$

for bedrock. K_s and K_r $[L^{-1}]$ are erodibility constants for sediment and rock, respectively. n is a constant set to 1 for all simulations in this paper, but that need not be 1 for the SPACE model in general. There are a variety of ways to compute water discharge q. We use the common approach of calculating discharge as a function of drainage area such that $q = k_q A^m$, where m is a scaling exponent and k_q is a coefficient subsumed into the fluvial erosion coefficients K_s and K_r.

Sediment deposition is implemented ~~similar~~ similarly to Davy and Lague (2009) such that the deposition flux depends on sediment flux Q_{sfluv} divided by the volumetric water discharge Q $\left[L^3/T\right]$ and the effective sediment settling velocity V $[L/T]$:

$$D_{s s_{fluv}} = \frac{Q_{sfluv}}{Q} V. \tag{5}$$

V is the net effective settling velocity, which represents the still-water particle settling velocity corrected for the upward effects of turbulence and the vertical gradient in sediment concentration through the water column (Davy and Lague, 2009). HyLands enables spatially variable values for V to distinguish between settling velocities in flooded and non-flooded areas.

2.2 Landsliding

HyLands treats landslide erosion and deposition deterministically, but uses a stochastic approach to calculating landslide occurrence. HyLands simulates deep-seated gravitational landslides eroding simultaneously the sediment layer and the bedrock (erosion terms $E_{s_{hill}}$ and $E_{r_{hill}}$ respectively in Eq. 1). We assume that both the rock and the sediment layer behave as Mohr-Coulomb materials. In its current form, HyLands does not simulate shallow landslides where failure geometry is imposed by the depth and angle of soil-rock transitions. Landslide initiation does not involve a preceding triggering event (e.g. an earthquake) but is simulated using a probabilistic approach.

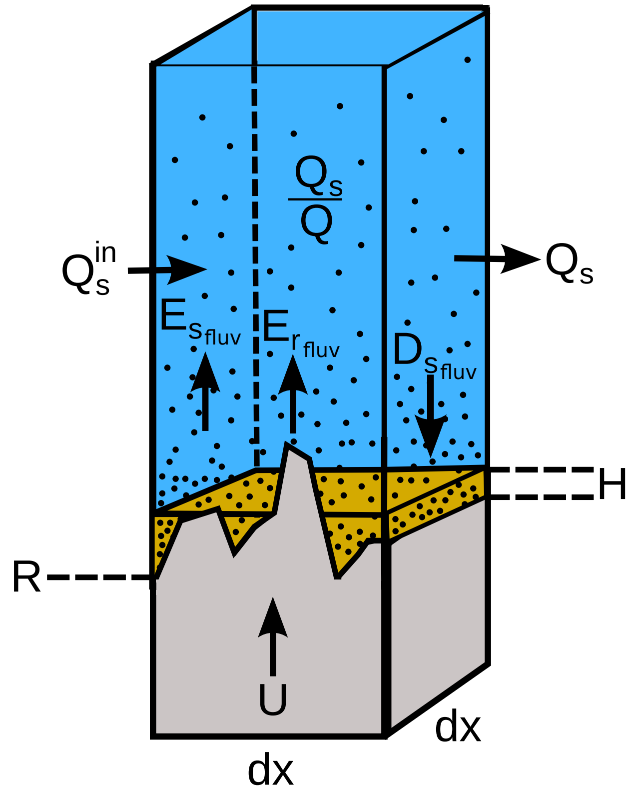

Figure 1. Sketch of fluvial SPACE component. Model setup and variable definitions for the SPACE bedrock-alluvial river erosion model. ~~Reproduced from Shobe et al. (2017).~~ Entrainment and deposition of sediment, as well as erosion of bedrock, can occur simultaneously. This approach allows channels to dynamically transition among bedrock, bedrock-alluvial, and fully alluviated states. At a given stream power, the relative ~~rate~~ rates of sediment entrainment $E_{s_{fluv}}$ and bedrock erosion $E_{r_{fluv}}$ ~~is~~ are set by the ratio of sediment thickness H to the bedrock roughness height H_* (Fig. 2). Modified from Shobe et al. (2017).

2.2.1 Landslide erosion

Following Densmore et al. (1998), we simulate landslide erosion using the Culmann theory for slope stability. Culmann (1875) proposes that hillslope failure will occur on the plane where the shear stress is balanced by the sliding resistance. Assuming Mohr-Coulomb materials, it has been shown that the failure plane with a dip θ_c bisects the local topographic slope β, and the material's angle of internal friction ϕ (Densmore et al., 1998; Champel, 2002):

$$\theta_c = \frac{\beta + \phi}{2}. \qquad (6)$$

The implementation of the Culmann theory in HyLands is illustrated in Fig. 3. For all points within the landscape where a landslide is initialized, the failure plane dipping at θ_c is extended until it daylights (i.e., intersects the topographic surface).

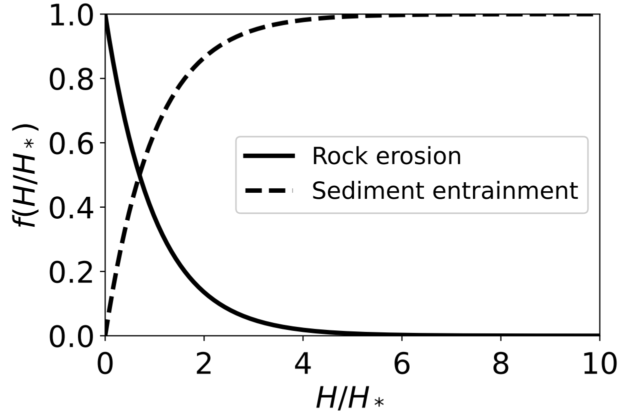

Figure 2. Relative efficiency of fluvial sediment entrainment and bedrock erosion ($f(H/H_*)$) as a function of the ratio of sediment thickness to bedrock roughness H/H_*. $f(H/H_*)$ depends only on the ratio H/H_*, and varies between 0 and 1, and indicates the proportion of total stream power used to erode bedrock entrain sediment (solid Equation 3; $f(H/H_*) = 1 - e^{-H/H_*}$; dashed line) or sediment erode bedrock (dashed Equation 4; $f(H/H_*) = e^{-H/H_*}$; solid line). As sediment thickness H increases relative to the bedrock roughness length scale H_*, the sediment entrainment rate factor approaches 1 and the bedrock erosion rate factor approaches 0 because the bed becomes composed entirely of sediment and no bedrock is exposed. As sediment thickness declines relative to the bedrock roughness length scale, the bedrock erosion rate increases exponentially because more bedrock is exposed and the sediment entrainment rate declines exponentially due to a lack of available sediment. This approach implements the "cover effect," in which the presence of sediment reduces bedrock erosion rates, but does not incorporate the "tools effect," in which mobile sediment enhances bedrock erosion. Reproduced Modified from Shobe et al. (2017).

Modeling andslide landslide frequency and location depends critically on the identification of points in the landscape where landslides initiate. A wide variety of events ranging from co-seismic activity and peak ground acceleration (Meunier et al., 2007) over intense storm events (Marc et al., 2018) to human hillslope destabilisation (Guns and Vanacker, 2014) may trigger mass wasting through landslide activity. Although these triggers could be added, HyLands mainly aims to simulate the impact of topographic landscape configuration on landslide activity. Therefore, we follow Densmore et al. (1998) in identifying unstable grid nodes cells as points in the landscape where the topographic slope (β) exceeds the angle of internal friction (ϕ). For all unstable nodescells, the probability for sliding, p_{LS}, is calculated as:

$$p_{LS} = \frac{H_s}{H_c}. \tag{7}$$

where H_s is the local hillslope height calculated as difference between every pixel cell in the landscape and it's its highest neighbour (Fig. 3) and H_c is the maximum stable hillslope height which is calculated as (Densmore et al., 1998; Champel, 2002):

$$H_c = \frac{4C}{\rho g} \frac{sin\beta \, cos\phi}{1 - cos(\beta - \phi)}. \tag{8}$$

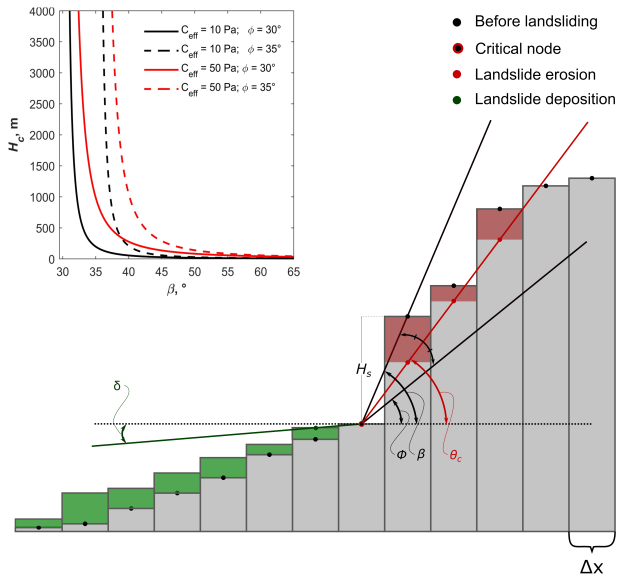

Figure 3. Sketch of landslide algorithm in two dimensions. Landslide erosion (red shaded area) is calculated using the Culmann approach (Culmann, 1875). β is the topographic slope, ϕ represents the angle of internal friction and θ is the inclination of the rupture plane. Deposition of landslide-derived sediment (green shaded area) is calculated using a non-local diffusion equation ~~(Eq. 11, cfr. Carretier et al., 2016)~~ (Eq. 11, cf. Carretier et al., 2016). δ is the minimal deposit surface angle ~~of the spreading slope under~~ at which landslide-derived sediment is distributed on the hillslope. This sketch illustrates a case where none of the landslide-derived sediment is in permanent suspension ($F_{f_{hill}} = 0$) and the amount of eroded sediment (red shaded area) equals the amount of deposited sediment (green shaded area). If the deposited volume creates a down-slope gradient which is lower than ~~the minimum spreading angle,~~ δ, the slope of the deposited volume is adjusted so that the ~~spreading slope~~ deposit surface angle equals δ. Probability for sliding is calculated as the ratio of the local hillslope height H_s to the maximum hillslope height H_c ~~(Eq. 7, cfr. Densmore et al., 1998)~~(Eq. 7, cf. Densmore et al., 1998). The inset plot illustrates that H_c depends on the rock strength (cohesion C and internal friction angle ϕ) and the topographic slope β. The plotted lines are calculated using Eq. 8 with ρ is 2700 $\mathrm{kg\,m^{-3}}$, and g = 9.81 $\mathrm{m\,s^{-2}}$.

Here C is the cohesion [$\mathrm{M\,L^{-1}\,T^{-2}}$], ρ is the rock density [$\mathrm{M\,L^{-3}}$] set to 2700 $\mathrm{kg\,m^{-3}}$, and g the gravitational acceleration (g = 9.81 $\mathrm{ms^{-2}}$). To simulate the random nature of landslides, grid ~~nodes~~ cells where landslides initiate are selected using a stochastic sampling scheme:

$$rnd\,\frac{dt}{t_{LS}}\begin{cases} > p_{LS} & \text{No Landsliding} \\ < p_{LS} & \text{Landsliding, select as critical cell} \end{cases} . \tag{9}$$

where rnd is a random number between 0 and 1 and t_{LS} is the return time for landslides with $t_{LS} >= dt$ ~~. Unstable nodes where~~ where dt is the model timestep. Unstable cells where a landslide is induced will further be referred to as critical ~~nodes~~ cells (Fig. 3). Every model iteration, Eq. 9 is updated for all ~~nodes~~ cells where the topographic gradient (β) exceeds the critical material friction angle (ϕ). From Eqs. 8 and 9, it follows that the probability for sliding depends on the topographic slope, β, and inversely correlates with the angle of internal friction, ϕ, and the cohesion of the material, C (see inset of Fig. 3). Cohesion is a scale-dependent variable and parameter values covering several orders of magnitude have been reported (Sidle and Ochiai, 2006). Jeandet et al. (2019) inverted several landslide inventories and found effective cohesion values ranging between 10 - 35 kPa. These values are lower than geomechanical values representing large-scale rock strength (e.g. Densmore et al., 1998; Champel, 2002) which is attributed to the decrease in rock cohesion in the vicinity of faults following earthquakes (Gallen et al., 2015). In our experiments, we will use values for cohesion in the range reported by Jeandet et al. (2019), which represent effective cohesion following an earthquake or a storm.

The landslide return time t_{LS} controls the absolute number of critical ~~nodes~~ cells where landslides are initiated. If t_{LS} equals the timestep dt, the number of landslides per timestep is solely controlled by the ratio H_s/H_c. When $t_{LS} >> H_s/H_c$, however, the number of landslides per timestep is reduced (Eq. 9). While the H_s/H_c ratio controls the topographic location of landsliding onset and thus the landslide characteristics (size and volume), the landslide return time ~~,~~ t_{LS} controls the absolute number of landslides and therefore overall landslide erosion rates.

HyLands enables the simulation of landslides at every location in the landscape. Every iteration, landslides are induced at critical ~~nodes~~ cells sampled using the probabilistic approach outlined above (Eq. 9, Figs. 3 and 4). We propose a recursive approach to calculate the magnitude of a single landslide. For every critical ~~node~~cell, we build a stack of unstable (= sliding) ~~nodes~~cells. The stack is initialized by adding the critical ~~node~~cell. Next, a recursive procedure is applied until the stack is empty. This procedure exists of the following steps: (i) Select the first ~~node~~ cell from the stack (thus starting with the critical ~~node~~cell). (ii) Evaluate all up-slope neighbouring ~~nodes~~cells. If the elevation of a neighbouring ~~node~~ cell exceeds the elevation of the sliding ~~plain~~ plane defined by θ_c, the ~~node~~ cell is identified as a sliding ~~pixel~~ cell and added the to stack of landslide ~~pixels~~cells. (iii) Remove the first ~~node~~ cell from the stack. This procedure is repeated until the stack is empty. HyLands offers the possibility to set a maximum landslide area ($A_{LS_{max}}$). Once this maximum is achieved, or when no more ~~pixels~~ cells are added to the stack of landslide ~~pixels~~cells, the landslide area is defined. All ~~pixels~~ cells inside this area are eroded to the elevation of the sliding plane, thereby adjusting both $E_{s_{hill}}$ and $E_{r_{hill}}$ of Eq. 1 for all ~~pixels~~ cells involved.

2.2.2 Flux of ~~landslide derived~~ landslide-derived sediment

The spatial change in ~~hillslope derived~~ hillslope-derived volumetric sediment flux $Q_{s_{Hill}}$ $[L^3/T]$ per unit width w $[L]$ is written as:

$$\frac{\partial (Q_{s_{Hill}}/w)}{\partial x} = E_{s_{hill}} + (1 - F_{f_{hill}})\, E_{r_{hill}} - D_{s_{hill}}. \tag{10}$$

where $F_{f_{hill}}$ is a unitless fraction of fine hillslope derived sediment. The factor $1 - F_{f_{hill}}$ $[-]$ represents the idea that some fraction of the hillslope derived sediment is instantaneously evacuated as ~~dissolved or~~ suspended sediment (Page et al., 1999; Hovius et al., 2000; Lin et al., 2008; Tenorio et al., 2018), and therefore should not be tracked as sediment. When $F_{f_{hill}} = 0$, the system is fully mass conservative and all sediments produced by landslide activity contribute to the sediment flux (Eq. 1).

2.2.3 Deposition of landslide material

In HyLands, landslides can initiate at any point in the landscape (Fig. 4). A steepest descent flow routing algorithm is known to be unrealistic for flow and sediment redistribution on hillslopes (Pelletier, 2010). Moreover, the use a constant spreading slope, as suggested by Densmore et al. (1998) does not take into account the topographic relief when redistributing landslide derived sediment. When using a constant sediment spreading slope, sediment deposited on flat parts of the landscape is spread out over a much longer distances than sediment deposited on steep parts~~, where the the large difference between topographic slope and spreading slope can accommodate for large sediment volumes~~. This is not realistic as sediment travel distance should depend on topographic gradient: material traveling over steeper slopes should go farther, all else being equal (Roering et al., 1999; Campforts et al., 2016).

A common approach to simulate sediment transport and deposition on hillslopes while considering the topographic gradient, is the use of linear or nonlinear diffusion equations (Roering et al., 1999; Andrews and Hanks, 1985). However, such an approach is not suited to simulate the distribution of landslide-derived sediment. While diffusion equations distribute sediment only between the neighbouring cells of a ~~pixel, landslide derived~~ cell, landslide-derived sediment has run-out distances which can be significantly longer than a single grid cell (Claessens et al., 2007). Therefore, we adopt a non-linear, non-local deposition scheme for landslide derived sediment outlined by Carretier et al. (2016):

$$D_{s_{hill}} = \frac{Q_{s_{Hill}}/w}{L} \tag{11}$$

where $D_{s_{hill}}$ $[L/T]$ is the volumetric deposition flux of hillslope derived sediment per unit bed area and L [L] represents a sediment transport distance. The larger L, the bigger the distance over which sediments are transported and the lower the local deposition rate. L is calculated for every grid cell as:

$$L = \frac{dx}{1-\left(\frac{S}{Sc}\right)^2} \tag{12}$$

where S_c is a critical slope, which we ~~furhter~~ further assume to be equal to the angle of internal friction (ϕ). When the hillslope gradient $S << S_c$, most of the incoming sediment will be deposited and the resulting outcome is similar to the one obtained using a regular diffusion equation, also referred to as a local solution (Furbish and Roering, 2013; Carretier et al., 2016). When S approaches S_c, L goes to infinity implying that no deposition will occur at the considered cell. At steep slopes, sediment transport therefore shows non-local behaviour in the sense that erosion ~~activity~~ of non-local, upstream cells is integrated when calculating the sediment flux Q_s (Carretier et al., 2016). When $S > S_c$, L is set to inf and there is no deposition at that cell. For negative values of S, which might occur for flooded ~~nodes~~cells, L is set to dx. In HyLands, a minimal ~~spreading~~ deposit surface angle (δ) can still be imposed under which ~~landslide derived~~ landslide-derived sediments are deposited but is not required (Fig. 3).

Contrary to ~~fluvial dynamics~~ the fluvial component of the model (SPACE) where a single flow direction algorithm (steepest descent) is used, landslide-derived sediment is spread over the ~~hillslopes~~ landscape using a multiple flow direction algorithm redistributing sediment over the downstream cells in proportion to the local slope ~~(Fig. 4, cfr. Carretier et al., 2016)~~

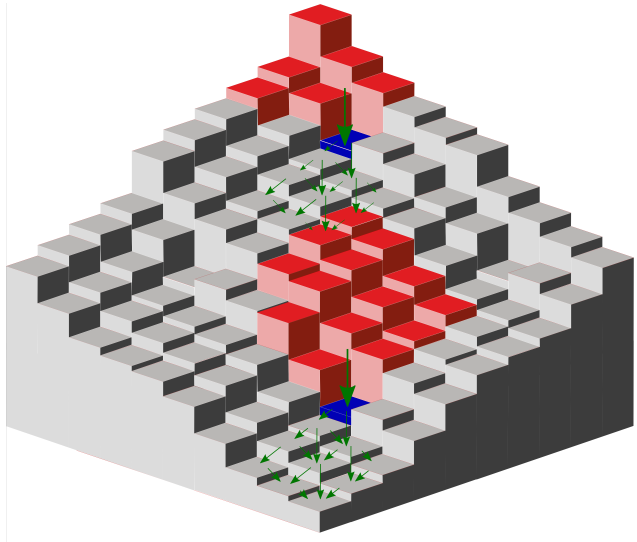

Figure 4. Sketch of landslide algorithm in three dimensions. Cells shaded in blue indicate the critical ~~nodes~~ cells where landslides potentially initiate. Cells shaded in red represent the landslide source areas. After mass failing, sediment will be redistributed over the downslope cells using a multiple flow direction algorithm (indicated with green arrows). Sediment deposition rate depends on a transport distance L (~~cfr~~cf. Eqs. 11 and 12).

(Fig. 4, cf. Carretier et al., 2016). When a lot of sediment is debouched into fluvial channels, rivers can be blocked by landslide dams. HyLands uses a lake identification algorithm to identify flooded ~~nodes~~ cells during every model iteration. Lakes are identified by filling all sinks in a landscape to the brim (Schwanghart and Scherler, 2014). By default, flooded ~~nodes~~ cells do not erode but do allow for sediment deposition (Eq. 5).

In the remainder of this paper, we will first evaluate the performance of the fluvial and landslide components of HyLands through a set of verification and validation runs. Next, the coupling between landslide activity and long term landscape evolution will be evaluated using a synthetic model setup where a steady-state landscape is exposed to a pulse of landslides. All model experiments executed in the framework of this paper are available as executable Matlab scripts and as dynamic landscape evolution movies (Table 2).

3 Verification and evaluation

3.1 Comparison to analytical solutions for the fluvial ~~dynamics~~component

In the first three test runs (detachment, transport-limited and mixed), a steady-state artificial landscape is simulated using a square grid of 20 by 20 ~~nodes with a coarse~~ cells with a spatial resolution of 100 m. The run is initialized from a surface with randomly generated microtopography. The initial surface is a tilted ~~plain~~ plane which drains towards the southwestern corner, the only open boundary ~~node~~cell. Therefore sediment and water can only leave the domain through this southwestern

Table 1. Parameter values

	No Landsliding			Landsliding				
	Detachment-limited	Transport-limited	Mixed	Namche-Barwa	Synthetic[a]			
					~~Pre~~	Pre	LS-Event	Po
Number of rows (−)	20	20	20	1918		75		
Number of columns (−)	20	20	20	1149		75		
~~Node~~ cell spacing (m)	100	100	100	20		20		
Time step (yr)	10	10	10	5		5		
Run time (kyr)	100	100	200	500	~~5×10^6~~	5×10^6	100	5×
Computation time per iteration[b] (s)	0.02	0.02	0.02	6.5		0.03	0.06	0.
Initial H (m)	0	100	0	0	~~0~~	0	varying	vary
~~U (myr^{-1})~~ U (m yr^{-1})	1×10^{-4}	1×10^{-4}	1×10^{-4}	0		1×10^{-3}		
K_r (m^{-1})	1×10^{-3}	1×10^{-4}	5×10^{-3}	5×10^{-4}		5×10^{-5}		
K_s (m^{-1})	0.01	0.01	0.01	1×10^{-3}		7.5×10^{-5}		
m (−)	0.5	0.5	0.5	0.5		0.5		
n (−)	1	1	1	1		1		
H_* (m)	1	1	1	2		.5		
ϕ_{sed} (−)	0	0	0	0		0		
$F_{f_{fluv}}$ (−)	1	0	0	0		0		
~~$V^{(b)}$ (myr^{-1})~~ V^c (m yr^{-1})	1	5	5	2		2		
~~$V^{(b)}_{Lake}$ (myr^{-1})~~ V^c_{Lake} (m yr^{-1})	1	5	5	10		10		
C (kPa)	-	-	-	15	~~-~~	-	15	-
ϕ (°)	-	-	-	38	~~-~~	-	35	-
t_{LS} (yr)	-	-	-	2×10^4	~~-~~	-	2×10^3	-
δ (°)	-	-	~~0.01~~ -	0.01		-	0.01	-
$F_{f_{hill}}$ (−)	1	0	0	0.25	~~-~~	-	0.25	-

Not all parameters will influence the model outcome in all cases. For example, the value of V is irrelevant for the detachment-limited case when all eroded bedrock passes out of the model domain a permanently suspended fine sediment ($F_{f_{fluv}} = 1$). Landslide parameters are only relevant for models where landslide activity is simulated.

[a] The synthetic landscape evolution model consists of three stages: a pre-landslide stage, a landslide stage and a post-landslide stage. Only parameter values which differ for these stages are listed i table.

[b] Time spent to complete one full model iteration on a windows PC, with an Intel(R) Core(TM) i9-9880H CPU @ 2.30GHz and a RAM of 32GB.

[c] HyLands enables spatially variable values for V (Eq. 5) to distinguish between settling velocities in non-flooded versus flooded cells by changing the values for V and V_{Lake}, respectively.

corner. The setup is identical to the one proposed by Shobe et al. (2017) in order to facilitate comparison. The timestep is set to 10 years. Under detachment-limited conditions (imposed by setting $F_f = 1$), the sediment thickness H equals 0 everywhere ~~and~~ through the entire model run and sediment produced by river incision into bedrock is instantaneously evacuated from the simulated domain. When assuming that water discharge is proportional to the drainage area ($q \propto A^m$) it has been shown that

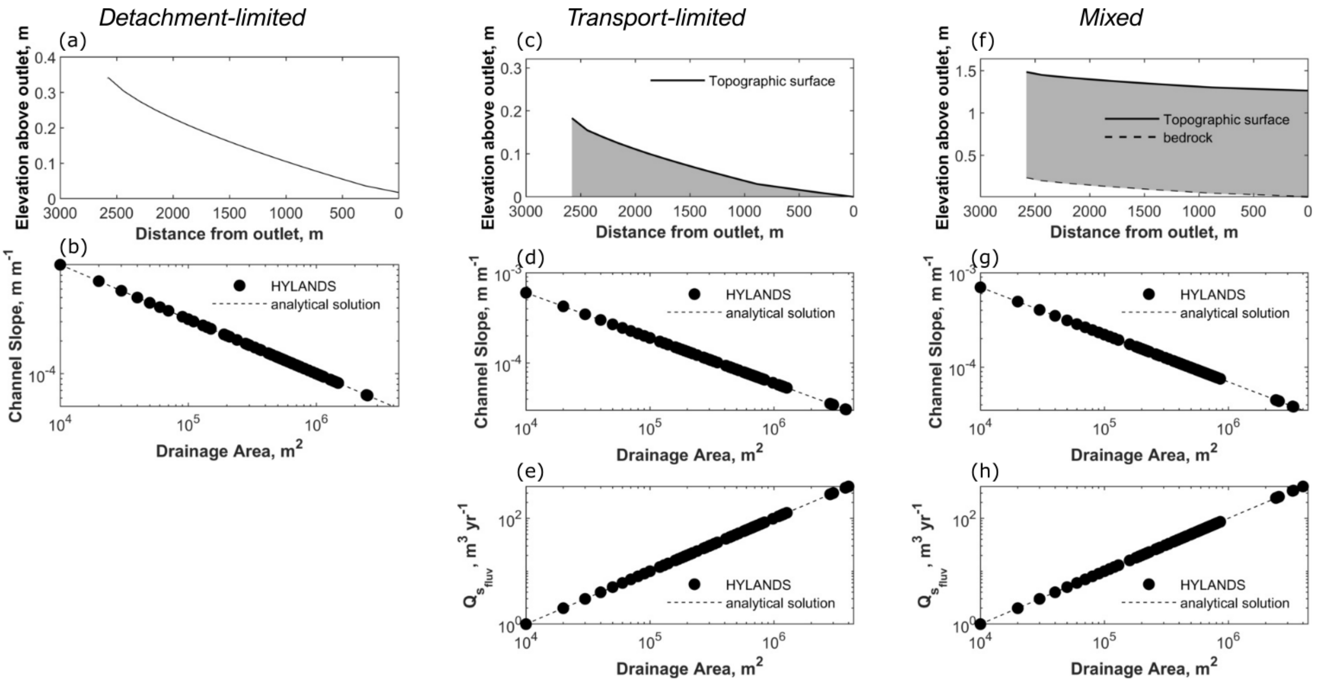

Figure 5. Verification of fluvial SPACE component. **(a)** Longitudinal profile of the trunk stream at steady state ~~simulated~~ under detachment-limited conditions where no sediment is present because $F_{f_{fluv}} = 1$ and all produced sediment is assumed to be evacuated instantaneously. At steady state, the ~~profile evolves towards a~~ concave-upward profile ~~, being~~ is in equilibrium with the imposed rock uplift ~~which is reflected in the~~ pattern. The steady-state slope-area relationship **(b)** ~~matching~~ matches the ~~predicted~~ analytical solution (Eq. 13). **(c)** Longitudinal profile of the trunk stream at steady state ~~simulated~~ under transport-limited conditions. At steady state, the ~~profile evolves towards a~~ concave-upward profile ~~, being~~ is in equilibrium with the imposed rock uplift ~~which is reflected in the~~ pattern. The steady-state slope-area relationship **(d)** ~~matching~~ matches the ~~predicted~~ analytical solution (Eq. 14). **(e)** illustrates the steady-state fluvial sediment flux $(Q_{s_{fluv}})$ as a function of the drainage area~~and~~ , which matches ~~with~~ the ~~predicted~~ analytical ~~flux-area~~ area-flux relationship (Eq. 15). **(f)** Longitudinal profile of the trunk stream at steady state ~~simulated~~ under mixed ~~alluvial-bedrock~~ bedrock-alluvial conditions. At steady state, both the topographic and bedrock profiles are in equilibrium with the imposed rock uplift ~~which is reflected in the~~ pattern. The steady-state slope-area relationship **(g)** ~~matching~~ matches the ~~predicted~~ analytical solution (Eq. 16). **(h)** illustrates the steady-state fluvial sediment flux $(Q_{s_{fluv}})$ as a function of the drainage area~~and~~ , which matches ~~with~~ the ~~predicted~~ analytical ~~flux-area~~ area-flux relationship~~under hybrid sediment-bedrock fluvial incision dynamics~~ . (Eq. 15).

~~under steady-state conditions,~~ fluvial erosion results in the following steady-state slope-area relationship (Shobe et al., 2017):

$$S = \left(\frac{U}{K_r A^m}\right)^{1/n}. \tag{13}$$

Fig. 5.b illustrates that when using parameter values listed in Table 1, HyLands reproduces the slope-area relationship given by Eq. 13. Similarly, it can be shown that under transport-limited ~~configurations~~ conditions where $H >> H_*$, the theoretical

slope-area relationship for fluvial incision can be written as (Shobe et al., 2017):

$$S = \left[\frac{V}{r} + 1\right]^{1/n} \left[\frac{U}{K_s}\right]^{1/n} A^{-m/n}, \tag{14}$$

where r represents the runoff rate $[L/T]$. To mimic a ~~transport limited~~ transport-limited configuration, we run HyLands assigning an initial sediment thickness H of 100 m. Other parameters values are shown in Table 1. Figure 5.d illustrates the slope-area plot for all ~~nodes~~ cells of the simulated steady-state landscape showing a close match with the analytical prediction (14). Moreover, HyLands also reproduces the theoretical steady-state sediment flux relationship for transport-limited conditions (Shobe et al., 2017):

$$Q_{S_{fluv}} = UA. \tag{15}$$

Finally, we evaluate the hybrid nature of the SPACE component in simultaneously simulating fluvial bedrock incision and sediment dynamics. Under such ~~configuration~~ conditions the slope-area relationship can be written as (Shobe et al., 2017):

$$S = \left[\frac{UV}{K_s A^m r} + \frac{U}{K_r A^m}\right]^{1/n}. \tag{16}$$

~~Under~~ At steady-state, both the height of the bedrock and the sediment layer should remain unchanged so that:

$$\frac{\partial \eta}{\partial t} = \frac{\partial R}{\partial t} + \frac{\partial H}{\partial t} = 0 + 0 = 0 \tag{17}$$

which leads to a constant soil thickness over the landscape ~~given~~ derived by (Shobe et al., 2017):

$$H = -H_* ln\left[1 - \frac{V}{\frac{K_s r}{K_r} + V}\right]. \tag{18}$$

To evaluate the performance of the hybrid fluvial dynamics, we run HyLands to a steady-state, starting from an initial surface without any sediment cover and using parameter values listed in Table 1. The obtained slope-area relationship (Fig. ~~2~~5.g) matches with the theoretical relationship Eq. 16, so does the soil thickness H which evolves toward a constant thickness (Eq. 18) and the sediment flux relationship honoring (Eq. 15).

3.2 Evaluation of the landslide component

Because ~~landslide activity~~ landsliding is a stochastic process, it not possible to derive an exact, analytical, solution to evaluate the performance of the landslide component in HyLands. However, it has been shown that most landslide inventories obey consistent magnitude-frequency and magnitude-volume relationships (Malamud and Turcotte, 1999; Stark and Hovius, 2001; Guzzetti et al., 2002; Korup, 2005; Guns and Vanacker, 2014; Larsen and Montgomery, 2012). To evaluate the performance of HyLands, we run the model over a limited amount of time for an area where both relationships are well constrained. The performance of the landslide module is evaluated based on its capacity to reproduce those calibrated relationships.

3.2.1 Landslide scaling relationships

A first empirical universal relationship is the landslide magnitude-frequency distribution that describes the number of landslide events of a given size. This relationship is characterized by a negative power law for landslides having an area greater than a given threshold value and a characteristic rollover for smaller landslides (Stark and Hovius, 2001; Malamud and Turcotte, 1999; Guzzetti et al., 2002). Magnitude-frequency distributions are typically described using a three parameter inverse gamma distribution as (Malamud et al., 2004):

$$p(A_L;\rho_l,a_l,s_l) = \frac{1}{a_l * \Gamma(\rho_l)} \left[\frac{a_l}{A_L - s_l}\right]^{\rho_l+1} exp\left[\frac{a_l}{A_L - s_l}\right] \tag{19}$$

where A_L is the landslide area $\left[L^2\right]$, $p(A_L)$ is the probability density of a landslide area (A_L), a_l, s_l and ρ_l are empirical parameters, and $\Gamma(\rho_l)$ is the gamma function of ρ_l. A second empirical universal relationship, is the volume-area scaling relationship where the volume V_L of a given landslide is a function of its area A_L as (Hovius et al., 1997):

$$V_L = \alpha_l A_L^{\gamma_l} \tag{20}$$

where α_l is an intercept and γ_l a scaling exponent.

3.2.2 Applying HyLands to the Namche Barwa-Gyala Peri massif

To evaluate to the performance of HyLands, the model is applied to a digital elevation model (DEM) of the Eastern Himalaya where the Yarlung Tsangpo river cuts through the Namche Barwa-Gyala Peri massif (Fig. 6). The area is characterized by rapid exhumation (King et al., 2016), steep topography, and steep river gradients causing high stream power (Finnegan et al., 2008). To quantify erosion rates in the area, Larsen and Montgomery (2012) mapped more than 15,000 landslides and constructed an inventory of landslides pre-dating 1974 and an inventory containing all landslide events between 1974 and 2007 (Fig 8.a). We use this area solely to demonstrate and evaluate the performance of HyLands and do not aim to reproduce exact features of landscape exhumation in this region. We selected the Namche Barwa-Gyala Peri massif to evaluate the performance of HyLands given its unique geomorphologic configuration featuring amongst the highest globally documented river stream power in combination with very active hillslope processes (Larsen and Montgomery, 2012). With HyLands being designed to couple the role of fluvial and hillslope processes, this region makes up for a good test environment. Note however that we do not intent to calibrate neither validate the model but run it using fixed, theoretical model parameters (section 3.2.3). Applications of HyLands aiming to constrain the model through parameter calibration and validation (section 4.3) would require additional data to ground-truth landslide inventories and to provide detailed records on landslide triggers such as earthquakes and storms.

3.2.3 Model parameterization

We run HyLands using the NASA Shuttle Radar Topography Mission (SRTM) v3.0 elevation data as an initial surface (Farr et al., 2007), resampled to a higher resolution of 20 m using a bicubic interpolation method. We resampled the DEM to

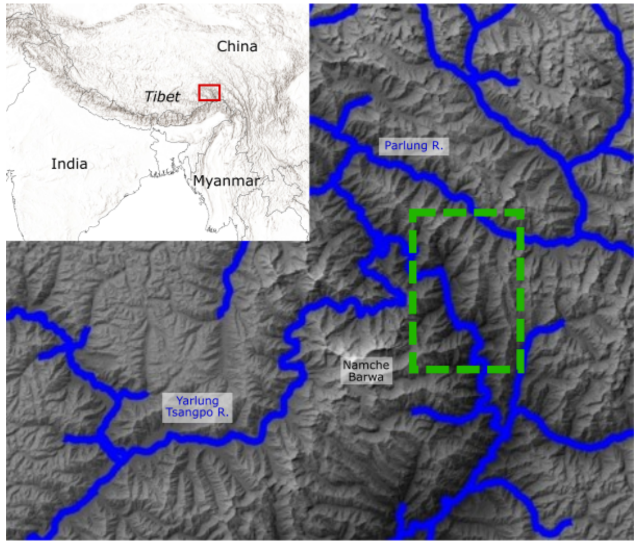

Figure 6. Namche Barwa-Gyala Peri massif used for model evaluation. The red rectangle on the inset figure indicates the ~~geographical~~ location of the study area. The green dashed rectangle indicates the part of the DEM used to evaluate HyLands. The shaded colours ~~indicate elevations, which were~~ show elevation derived from the 30 m SRTM v3 DEM ~~(?)~~ (Farr et al., 2007) and resampled to a higher resolution of 20 m using a bicubic interpolation method. Main map is produced with TopoToolbox (Schwanghart and Scherler, 2014). Inset map is made in QGis 3©, using Natural Earth vector and raster map data available at www.naturalearthdata.com.

a resolution of 20 m in order to evaluate the capacity of HyLands to reproduce the rollover in the magnitude frequency distribution, often reported to occur for landslide areas < 900 m^2, which would be the minimum landslide area when using the original SRTM data. As shown in Fig. 6, we only simulate part of the larger Namche Barwa-Gyala Peri massif studied by ~~(Larsen and Montgomery, 2012)~~Larsen and Montgomery (2012). We selected a region mostly free of glaciers and surrounding the section of the Yarlung Tsangpo river where unit stream power is very high (ranging between 500 - 4000 W.m^2, (Finnegan et al., 2008). The simulated grid is composed of 1918 $\times$ 1149 ~~nodes~~cells, covering a total area of ca. 960 km^2. We simulate landscape evolution over 500 years, using time steps of 5 years. For this experimental run, we assume that there is no uplift. We acknowledge that this condition is not met in the area, but imposing an uplift field is not necessary for evaluating the performance of the HyLands landsliding algorithm. Inserting realistic uplift patterns to simulate the dynamic evolution of the area would require (i) implementation of the complex tectonic configuration of the area (King et al., 2016) and (ii) simulation of a bigger area to capture the dynamic interplay between uplift and river dynamics. This is beyond the scope of the application and we therefore assume that the tectonic configuration controlling landscape evolution over the limited timescale simulated in this experiment (500 years) is captured by the topography of the area (Kirby and Whipple, 2012).

We run HyLands assuming open boundary conditions: all sediment produced within the domain through river incision and landsliding can be exported from the domain across any of the four boundaries. For simplicity, we use a simple stream power formulation for river incision where thresholds for both sediment entrainment and bedrock erosion are negligible. Standard

Table 2. Simulation movies and script names

			Script name on GitHub	Link to movie
No Landsliding	Detachment-limited		HyLands-NoLS-DL.m	https://doi.org/10.5446/45969
	Transport-limited		HyLands-NoLS-TL.m	https://doi.org/10.5446/45967
	Mixed		HyLands-NoLS-Mixed.m	https://doi.org/10.5446/45968
Landsliding	Real DEM, Namche-Barwa		HyLands-LS-NB.m	https://doi.org/10.5446/45973
	Synthetic	Before intense LS period	HyLands-LS-B-LS.m	https://doi.org/10.5446/45970
		intense LS period	HyLands-LS-LS.m	https://doi.org/10.5446/45971
		After LS period	HyLands-LS-A-LS.m	https://doi.org/10.5446/45972

scaling exponents are used ($m = 0.5$ and $n = 1$ in Eq. 4) and the bed sediment porosity and the fraction of fine river sediments are assumed to be zero ($\phi_{sed} = 0$ and $F_{f_{fluv}} = 0$ in Eq. 1). We calculate landslide activity using the landslide module of HyLands and assume that 25% of the landslide-derived sediment is evacuated out of the system as fine material ($F_{f_{hill}} = 0.25$). We assume that the angle of internal friction (ϕ) is comparable to the mode of the topographical slope distribution (Burbank et al., 1996; Korup, 2008; Montgomery and Gran, 2001), reported to range between 37°- 39° and here set to 38° (Larsen and Montgomery, 2012). Cohesion C is known to vary over a wide range and strongly depends on rock mechanical properties (Wyllie and Mah, 2017). Site-specific calibration would require detailed mapping of lithologcal units and we therefore set C to 15 kPa, a value in the range of previously optimized cohesion for the Himalaya ~~(Jeandet et al., 2019, 12-20Pa in)~~ (12-20 Pa in Jeandet et al., 2019). Cohesion and the angle of internal friction ~~influences the size-distribution~~ influence the size distribution of landslides in several ways (Jeandet et al., 2019). The angle of internal friction ϕ controls the angle of the potential rupture plane such that lower values of ϕ will result in lower rupture dipping angles, which, for the same topographical configuration, results in thicker and larger landslides. The effective rock cohesion value C influences the critical hillslope height H_c in Eq. 6. Larger values ~~values~~ for C will result in larger values for H_c, thus decreasing the probability of landslides on ~~less steep slope sections~~ gentler slopes and resulting in fewer small landslides. The minimum value of the ~~spreading slope~~ minimal deposit surface angle under which landslide-derived sediment is redistributed on hillslopes is set to 0.01°. We set the return time for landsliding t_{LS} to $2{\times}10^4$ years. t_{LS} regulates the probability that unstable cells evolve into a landslide (Eq. 9) and therefore controls the number of landslide events per timestep Δt. When applying HyLands to reconstruct or predict landslide activity, t_{LS} should be a function of the frequency (or return time) of triggering events (large earthquakes or rainfall events). Evaluation of model sensitivity to changing values for t_{LS} is a natural avenue for further work. A full overview of the model parameters is given in Table 1.

3.2.4 Model evaluation results

Figure 7 shows time slices of the model run after 5 (initial iteration), 165, 330 and 500 (final iteration) model years. Locations for landslide initiation (critical ~~nodes~~cells) are well spread over the landscape. The number of landslide events (the number of black ~~dots~~ diamonds in Fig. 7) is mainly controlled by the return time for landsliding t_{LS}. The fan-shaped deposition zones of landslide-derived sediments reflect the use of a multiple flow sediment routing algorithm. Landslide-derived sediment predominantly accumulates at hillslope toes, as well as in or near river channels. Some accumulation also occurs on hillslopes. Overall, landslides strongly influence the thickness of the alluvial bed sediment layer. Note that the shape of the erosion and deposition zones adjust through the course of the model run. The presence of previous landslide activity alters the topographic relief and hence determines which ~~pixels~~ cells become susceptible to erosion and deposition as landscape evolution continues (e.g., the deposition pattern in Fig. 7.h reflects the shape of erosion patterns resulting from previous landslide activity).

To quantitatively evaluate the performance of the HyLands landslide module, we compare modelled landslide properties against observed scaling relationships (Eq. 19 and 20). Figure 8.a compares the modelled and observed magnitude-frequency distribution. We observe good correspondence between the model and the data, with the power-law tail of the distribution falling within the envelope defined by the two inventories of Larsen and Montgomery (2012). Similarly to observed magnitude-frequency distributions, HyLands simulates the rollover or the transition from an increasing magnitude-frequency relationship to a decreasing one. This observation confirms that the shape of landslide magnitude-frequency distributions can be explained using mechanical landslide processes (~~cfr.~~ cf. Section 2.2.1) and the ~~geometry~~ topography of the studied region (Jeandet et al., 2019). Figure 8.b shows that HyLands is capable of approaching the ~~universal Area-Volume~~ shape of the universal area-volume relationships found by Larsen et al. (2010). While HyLands seems to overestimate simulated landslide volumes for very small landslides, the ~~fit between HyLands and the observed relationship improves for large landslides. We attribute overestimation of landslide volumes~~ Area-Volume relationship simulated with HyLands approaches a linear relationship in a log-log space for larger landslides, similar to the shape of the observed Area-Volume relationship. Note that overall, landslide volumes simulated with HyLands are over predicted compared to observations. Study-area-specific model calibration would improve this fit but is beyond the scope of this model evaluation in which we evaluate the capacity of HyLands to reproduce the shape of the universal area-volume relationship. We attribute the positive deviation from the linear Area-Volume relationship in a log-log space for smaller landslides to the nature of the landslide algorithm: ~~while HyLands~~ HyLands simulates deep-seated landslides, several of the smaller landslides are likely to be shallow landslides which are currently not simulated. Moreover, HyLands does not allow any sediment to be deposited within the landslide scar ~~,~~ while this typically does occur in nature. Future developments of the algorithm could allow for shallow landsliding and in-scar deposition for more realistic simulations. ~~Moreover~~Furthermore, there is a resolution effect: due to DEM noise or heterogeneity, the algorithm might select small landslides of one or two cells on very steep hillslope patches thus resulting in high landslide volumes. However, such steep hillslope patches might represent noise in the DEM rather than actual steep slopes. ~~The use of high resolution DEMs could partly resolve this issue.~~

3.3 Model application

The explicit coupling of landslides and landslide-derived sediment to long-term landscape evolution enables the study of a wide range of interactions which otherwise can only be inferred or partially simulated. A common application is to evaluate the coupling between landslides and river-bed morphology. To evaluate the impact of a landslide event on long-term channel profile evolution, we run a synthetic landscape evolution model to steady state. After 5 million years, we simulate a period of 100 years with intense landslide activity, analogous to a period of elevated landslide activity triggered by a series of seismic events. After 100 years of landslide activity, we assume that landslides are no longer triggered and let the landscape evolve back to its original steady state. Such an experiment not only allows evaluation of the extent to which landslides perturb the topography of river profiles, but also enables estimates of the time required for a landscape to respond to a major perturbation (e.g. a series of earthquake-triggered landslides).

The model run consists of three stages. In the first stage, the model is run to a steady state. For reasons of comparability, we simulate landscape evolution on a grid similar to the one used for the verification runs (section 3), i.e. with a single open boundary ~~node~~ cell in the southwestern corner. To simulate more realistic landscape scales, we use a domain of 75 by 75 ~~nodes~~ cells with a higher resolution of 20 m. A complete overview of model parameter values is given in Table 1. The evolution of the landscape over time is shown in a series of time slices (Fig. 9.a-c). Model behaviour at this stage is as expected for the SPACE river erosion model when hillslope processes are not explicitly simulated (Shobe et al., 2017). During the first timesteps, the drainage network establishes and the landscape gradually approaches a steady state with uniform sediment thickness across the entire landscape.

In the second stage (Fig. 9.d-f), we simulate a period of intense landslide activity by triggering a large number of landslides. Landslides are initiated based on their probability of sliding (Eq. 7) assuming an internal friction angle of 35° and a low landslide return time (t_{LS} = $2{\times}10^3$ years). Under this configuration, many of the steep portions of the landscape become prone to landslide erosion and transform into a landslide source area. We assume that 25% of the landslide-derived sediment is instantaneously evacuated out of the system as fine material ($F_{f_{hill}} = 0.25$). Landslides trigger the formation of landslide dams, resulting in flooded river sections. Landslide dams not only alter the topographic elevation of the simulated domain but also change the drainage network. The location of the river bed can change due to landslides and landslide-derived sediment rearranging the valley-bottom topography. ~~This is why the bedrock profile of the plots shown in Fig. 9.e-h has a bumpy shape at several locations along the profile.~~

Immediately after the intense landsliding period, the trunk stream of the drainage network is still choked with sediment and landslide dams are abundant (Fig. 10.a-f). In the first few thousand years following the intense landsliding period, the lakes gradually fill ~~in~~ with sediment. After 1500 years, most of the landslide-dammed lakes are filled with sediment. The fluvial profile is now characterized by a chain of knickpoints characteristic for fluvial profiles experiencing the delivery of ~~immobile~~ debris by landslides (Ouimet et al., 2007) or other hillslope processes (Shobe et al., 2016, 2018). Where the in-channel bedrock is not covered with sediment, river incision into bedrock continues. However, upstream of landslide dams, the bed is choked with sediment and the alluvial cover is too thick for bedrock incision to continue. As bedrock uplift continues and sediment is slowly been evacuated from evacuated from filled lakes, the bedrock profile adjusts and small knickpoints are created along the river profile. While the specific cause is different (landslide dams ponding sediment vs. delivery of large-grained colluvium), the mechanism of knickpoint generation is similar to the numerical simulations of Shobe et al. (2016) and Shobe et al. (2018) in that a bare-bedrock reach downstream of a sediment-mantled reach can undergo faster erosion, thereby generating knickpoints that are decoupled from the baselevel signal.

There are two distinct mechanisms for the generation of irregularities in the channel profiles: drainage re-routing due to landslide dams and knickpoint generation due to spatially varying sediment cover triggering differential erosion. The former mechanism can result in reaches where the bedrock slope is adverse relative to the water surface slope (the bumps in the bedrock profile in Fig. sFigs. 9 and 10). The latter creates variability in the magnitude, but not the direction, of the bedrock slope. The drainage re-routing mechanism dominates in the simulations presented here and results in the formation of epigenetic river gorges (Fig. 10). Epigenetic gorges are characterized by rivers incising into the bedrock of former valley walls due to the blockage of the formal channel by landslide-derived sediment (Ouimet et al., 2008).

4 Discussion

Landscapes are the outcome of external perturbations, such as climate or tectonic variability, and internal dynamics originating from the coupling between fluvial incision and hillslope response (Burbank and Anderson, 2011; Glade et al., 2019). Much effort has been devoted towards to understanding the relationship between fluvial erosion efficiency and climate variability both through theoretical developments (Tucker, 2004; Lague, 2014) and observations (DiBiase and Whipple, 2011; Ferrier et al., 2013). A main finding of those authors is that the role of allogenic fluvial response (i.e. transient adjustment to an external perturbation) can only be understood when considering autogenic fluvial dynamics such as the existence of incision thresholds (Snyder et al., 2003; Lague et al., 2005) and the internal lithological heterogeneity in a landscape (?Glade et al., 2019) (Campforts et al., 2020; Glade et al., 2019). However, the role of landslides in long-term landscape evolution, and especially the dynamic interaction between river incision and landslide activity, is only poorly understood. HyLands offers a tool to study dynamic feedbacks between landslides and river incision. The role of sediment dynamics in altering fluvial erosion and sediment transport is clearly illustrated in the numerical experiment (FigFigs. 9 and 10) where 5-10 kyr are required for the landscape to evolve back to a steady sate after a pulse of landsliding. Not only does the delivery of landslide-derived sediment to the channel bed alter the topography of the channel profile, it also results in the formation of bedrock knickpoints and associated retreating incision waves. HyLands thereby corroborate The HyLands output thereby corroborates earlier observations that landslides, and tight channel-hillslope couplings in general, are autogenic mechanisms altering the way in which landscapes respond to external (allogenic) perturbations (Ouimet et al., 2007; Shobe et al., 2016; Glade et al., 2019). HyLands is designed to study the dynamic feedbacks between landslides and river erosion at large spatial and temporal scales. To do so, the model integrates an algorithm for deep-seated landsliding with a recently proposed model for fluvial incision (Shobe et al., 2017). HyLands enables simulations over several millions of years and reproduces analytical predictions for fluvial dynamics and observed landslide scaling relationships.

4.1 Fluvial component

The SPACE river erosion model, which governs river evolution in HyLands, advances on existing river incision models in that it explicitly simulates the role of sediment in reducing the efficiency of bedrock incision (Beaumont et al., 1992; Lague, 2010). However, like SPACE, HyLands does not simulate the effect of increased bedrock incision efficiency due to mobile sediment acting as eroding tools (Sklar and Dietrich, 2004). Field observations warrant consideration of the tool effect (Cook et al., 2013; Beer et al., 2017), and theoretical predictions have shown that the interaction between sediment and bedrock incision is adjusted when the tool effect is considered (Gasparini et al., 2007). The impact of explicitly simulating the tool effect due to landslide-derived sediment has been evaluated in a numerical modelling study (Egholm et al., 2013). Egholm et al. (2013) concluded that landslide activity and its delivery of abrasive agents to the channel accelerate fluvial incision in actively uplifting mountain regions, whereas the lack of landslides in tectonically inactive mountain ranges strongly decreases erosion efficiency and enables topographic preservation. Adding the tool effect and evaluating its potential importance is therefore a primary goal for further model development in HyLands. Simulating the tool effect of sediments can be achieved by making the bedrock erosion function dependent (Eq. 4) on the sediment flux Q_s (cfr. e.g. Gasparini et al., 2007; Hobley et al., 2011) (cf. e.g. Gasparini et al., 2007; Hobley et al., 2011; Zhang et al., 2018).

Like SPACE, HyLands does not include process-based approaches (Kean and Smith, 2004; Wobus et al., 2006; Davy and Lague, 2009; Coulthard et al., 2013), simplified width adjustment rules (Lague, 2010; Yanites, 2018), or empirical closures (Attal et al., 2008) to dynamically calculate river width adjustments though time. HyLands assumes a relationship between drainage area and river width depending on the scaling exponent m (fixed in our simulations to 0.5; see also Table 1). This approach implies that all river cells in the landscape are assumed to occupy 1 grid cell with distance dx, that channel width may be less than, equal to, or greater than dx, and that river width is only a function of contributing drainage area. It has however been shown that river width might vary as a function of sediment flux or under varying tectonic configurations (Amos and Burbank, 2007; Turowski et al., 2009). Recent work using a 2D hydro-sedimentary numerical model (Davy et al., 2017) based on the Saint-Venant Equations equations has shown that river re-organisation and narrowing after landslide events might strongly increase sediment transport capacity and alter sediment evacuation time after big large landslide events (Croissant et al., 2017). While simulating dynamic river width reorganisation at the landscape scale is currently not possible over longer timescales due to computational limitations, generic approximations for the landslide triggered landslide-triggered channel narrowing (Croissant et al., 2019) could be integrated in future versions of HyLands.

4.2 Landslides

The landslide algorithm in HyLands is based on finite slope mechanics and assumes a planar rupture plane geometry. Although our approach reproduces observed magnitude-frequency and area-volume scaling relationships and is supported by previous work where landslides have been simulated using planar rupture planes surfaces (Jeandet et al., 2019), the use of more advanced rupture plane geometries has been proposed. ? Gallen et al. (2015) for example propose the use of concave-upward rupture planes to simulate co-seismic landsliding. However, their approach is based on the statistical aggregation of one-dimensional slope-stability solutions and therefore does not fully honor simplifies the three-dimensional topographic complexity of the topographic surfacelike HyLands does. Evaluating the role of varying rupture plane geometries in three dimensions is one of the potential future developments of HyLands.

At this stage HyLands does not explicitly simulate shallow landsliding, which typically occurs at the interface between the bedrock and the overlying sediment/regolith cover. Given the existing ability of HyLands to simultaneously simulate bedrock evolution and sediment thickness, adding a shallow landslide algorithm is feasible (Montgomery and Dietrich, 1994; Claessens et al., 2007) and would further our understanding of the coupling between climate variability and landscape stability (Parker et al., 2016). For shallow landslides to be added as a component in HyLands, the implementation and calibration of a regolith formation and soil flux model will however be required (Campforts et al., 2016). Using additional model components to simulate soil formation and transport requires calibration of several additional processes components; care is needed to prevent over-calibration and -parameterization of the model (Van Rompaey and Govers, 2002).

Our probabilistic sliding mechanism neglects seismic or hydrological landslide triggers (e.g. Keefer, 1984, 2002; Keefer and Larsen, 2007; Marc et al., 2015, 2018, 2019). Rather we simulate landslides as a stochastic process based on the mechanical stability of slope patches. Future developments could however adjust the spatial probability of landsliding by coupling an explicit earthquake model to HyLands (cfr., Croissant et al., 2019)(cf., Croissant et al., 2019). The probability for of co-seismic landslide activity can then be directly obtained by using constrained relationships between Peak Ground Acceleration peak ground acceleration (PGA) and landslide initiation probabilities (Meunier et al., 2007).

HyLands uses a non-linear, multiple-flow sediment redistribution scheme depending on topographic slope. Accurately simulating landslide sediment run-out distances is however a challenging process which is difficult to constrain and often simulated using empirical approximations (e.g. based on the absolute height difference within a landslide (Claessens et al., 2007)). A potential way to validate and calibrate landslide runout distance would be to compare landslide-derived sediment distributions simulated with HyLands with runout distances simulated with higher complexity models (Iverson, 2000; Iverson and George, 2016; Zhou e higher-complexity models (Iverson, 2000; George, 2011; Zhou et al., 2020) or medium-complexity approaches such as RAMMS or Flow-R (Horton et al., 2013; Fan et al., 2017). Nevertheless, in its current form, HyLands reproduces characteristics of landscapes and channel profiles dominated by deep-seated landslides (Ouimet et al., 2007), and is therefore a useful tool to study the interaction between river incision and landslide dynamics at landscape evolution space and time scales.

4.3 Calibration of HyLands

A main challenge when applying HyLands in real settings is the calibration of both the river incision and landslide parameters. The power of any LEM lies in its capacity to integrate data over multiple spatial and temporal timescales. Therefore, a range of datasets can be used to constrain model parameters. We identify three main categories of potential calibration data.

1. Topographic parameters that can be derived from DEMs. These include a range of metrics describing river characteristics (drainage density, river steepness, river stream power), hillslope properties (slope distribution, mean and median slope angels, aspect), and landslide scaling relationships (magnitude-frequency and area-volume distributions). All these

metrics can be derived from topographic data and subsequently used to constrain HyLands erosion parameters (~~cfr~~cf. Fig. 7).

2. Data directly constraining the the integrated effects of river incision or landslide erosion. Ongoing efforts to map mass movements in ~~landslide prone~~ landslide-prone areas now enable estimates of erosion rates over ~~decal~~ decadal timescales (Hovius et al., 1997; Larsen and Montgomery, 2012). Data on sediment redistribution following landslide events is however more difficult to collect Fan et al. (2019). Although initial compilations now exist of global landslide sediment mobilization rates (Broeckx et al., 2020), such inventories remain incomplete. Data on landslide mobilization rates can be used to train HyLands while in turn, HyLands can be used to further extend datasets on landslide mobilisation rates and predict landslide sediment production rates in regions which are otherwise difficult to access.

3. Catchment-averaged cosmogenic radionuclide (CRN) derived erosion rates. CRN data has been used to calibrate river incision models that explicitly integrate the stochastic nature of fluvial incision over time ~~(DiBiase and Whipple, 2011; Scherler et al., 2~~ (DiBiase and Whipple, 2011; Scherler et al., 2017; Campforts et al., 2020). However, CRN data is sensitive to landslide activity (Niemi et al., 2005; Yanites et al., 2009; Wang et al., 2017) and the calibration of stochastic river incision models has been shown to be sensitive to landslide activity ~~(?)~~(Campforts et al., 2020). HyLands directly simulates stochastic landsliding and hence enables explicit simulation of the impact of landsliding on CRN-derived erosion rates~~, making them a promising tool to constrain HyLands~~.

4.4 Potential applications

Given the capacity of HyLands to explicitly simulate the interaction between fluvial dynamics and landslide triggering, it provides a unique toolbox to advance the field of geomorphology on several fronts. In the following we outline two example applications.

First, HyLands can be used as an experimental environment to test how landslides influence landscape response to external perturbations. Landslides are known to mediate long term landscape evolution (Korup, 2005; Korup et al., 2007). By altering sediment fluxes, ~~they~~ landslides fundamentally alter the dynamic equilibrium between hillslopes and rivers, resulting in long-term implications for landscape evolution (Egholm et al., 2013). Moreover, large landslides are reported to critically alter drainage networks by causing major river captures (Korup et al., 2007; Dahlquist et al., 2018). A particular question which remains open for debate is the way in which landslides influence the evolution of a landscape to steady state. Although the stochastic nature of landslides prevents landscapes from evolving towards perfectly time- and space-invariant topographies, landslide-influenced landscapes will evolve towards a quasi-steady sate if external drivers such as climate and tectonics remain constant. Though the study of steady-state landscapes improves our mechanistic understanding of landscape evolution, an even more interesting and challenging question would be to study the impact of landslides on the dynamic evolution of a landscape towards such a steady state. The latter problem is more relevant for most real-world landscapes which are thought to be transient than in steady state (Mudd, 2017).

Second, HyLands can be used to evaluate the response ~~time~~ of a landscape to a ~~landslide~~ major landslide triggering event and to understand the timescales over which landslide-derived sediments are exported from the landscape ~~(Wang et al., 2015; Li et al., 2016; ?)~~ (Wang et al., 2015; Li et al., 2016; Schwanghart et al., 2016; Robinson et al., 2017; Roback et al., 2018). As illustrated in this paper, a landscape requires a certain response time to recover from a landslide event—or a series of landslide events—and to evolve back to a steady-state configuration (Fig. 10). Landslide activity is typically manifested in downstream sediment dynamics and LEMs are the right tool to simulate large-scale landscape response to landslide activity in upstream mountain regions. HyLands will enable prediction of downstream sediment response to landsliding, provided that the model can be calibrated effectively (section 4.3).

5 Conclusions

We presented a new, fully coupled model for river incision into bedrock, sediment transport, and bedrock landsliding. HyLands couples a mass conservative, sediment-flux-dependent ~~incision model (SPACE, Shobe et al., 2017)~~ river incision model (SPACE; Shobe et al., 2017) with a deep-seated landslide algorithm (Densmore et al., 1998) and a multiple-flow sediment redistribution algorithm (Carretier et al., 2018). HyLands is designed to simulate landscape evolution at large temporal and spatial scales. The fluvial component of the model matches known, steady-state analytical solutions developed in earlier work (Davy and Lague, 2009; Shobe et al., 2017). Landslides produced by HyLands replicate observed scaling relationships indicating the realism of the simulations. HyLands is implemented in the TopoToolbox GIS interface ~~(?)~~(Schwanghart and Scherler, 2014), thereby facilitating the use of rasterized field data for calibration and providing direct access to a wide range of GIS analysis tools. In an example application, we illustrated how HyLands can be used to evaluate the impact of landslide activity on fluvial and hillslope characteristics. We showed how landslide activity triggers the formation of landslide-dammed lakes and how HyLands is capable of simulating subsequent lake infilling and knickpoint formation, similar to reported landscape changes following landslide activity (Ouimet et al., 2007). The foremost advantage of HyLands is its capacity to explicitly simulate the role of landslides, landslide-derived sediment and fluvial dynamics at the landscape scale. The model is well-suited to address a range of new questions related to how channel-hillslope coupling modulates landscape ~~response to external~~ evolution and response to perturbations.

Code availability. The HyLands 1.0 TTLEM component as well as all other TTLEM components used in this paper are part of TopoToolbox version 2. The source code and future updates are available in the GIT repository: https://github.com/BCampforts/topotoolbox. The exact version of the software code used to produce the results presented in this paper is archived on Zenodo (https://zenodo.org/badge/latestdoi/78645261). Upon publication we will submit a pull request to the master repository where TopoToolbox is housed: (wschwanghart/topotoolbox). Documentation, installation instructions, and software dependencies for the HyLands project can be found at https://github.com/BCampforts/topotoolbox. Detailed scripts and user manuals for the simulations illustrated in this paper can be found at https://github.com/BCampforts/pub_hylands_campforts_etal_GMD which is also archived on Zenodo: https://zenodo.org/badge/latestdoi/247779084. HyLands is platform independent and requires MATLAB 2014b or higher and the Image Processing Toolbox. The HyLands modeling framework is distributed under a MIT open-source license.

Data availability. Digital elevation models used in this paper are derived from the 30 m SRTM v3 DEM (Farr et al., 2007). The resampled DEM is available through https://github.com/BCampforts/topotoolbox

Video supplement. Videos are described in Table 2 of the main text which contains hyperlinks to the following movies: https://doi.org/10.5446/45969; https://doi.org/10.5446/45967; https://doi.org/10.5446/45968; https://doi.org/10.5446/45973; https://doi.org/10.5446/45970; https://doi.org/10.5446/45971; https://doi.org/10.5446/45972

Author contributions. BC and CMS conceived the conceptual model on landslide-derived sediment dynamics and designed the research project. BC developed the algorithm with help from CMS. BC and CMS took the lead in writing the paper. Concepts to verify and evaluate model components were conceptualized by PS, DL, MVM and JB. All authors contributed to shaping the research, analyses, and paper.

Competing interests. The authors declare that they have no conflict of interest.

Acknowledgements. BC received funding from the Research Foundation Flanders, FWO grant agreement no. 12Z6518N. CMS received funding from the European Union's Horizon 2020 research and innovation programme under the Marie Skłodowska-Curie grant agreement no. 833132. PS and DL have received funding from the European Research Council (ERC) under the European Union's Horizon Horizon 2020 research and innovation programme (grant agreement no. 803721).

References

Amos, C. B. and Burbank, D. W.: Channel width response to differential uplift, Journal of Geophysical Research, 112, F02 010, https://doi.org/10.1029/2006JF000672, 2007.

Andrews, D. J. and Hanks, T. C.: Scarp degraded by linear diffusion: Inverse solution for age, Journal of Geophysical Research, 90, 10 193, https://doi.org/10.1029/JB090iB12p10193, 1985.

Armitage, J. J., Whittaker, A. C., Zakari, M., and Campforts, B.: Numerical modelling of landscape and sediment flux response to precipitation rate change, Earth Surface Dynamics, 6, 77–99, https://doi.org/10.5194/esurf-6-77-2018, 2018.

Attal, M., Tucker, G. E., Whittaker, A. C., Cowie, P. A., and Roberts, G. P.: Modelling fluvial incision and transient landscape evolution: Influence of dynamic Channel adjustment, Journal of Geophysical Research: Earth Surface, 113, 1–16, https://doi.org/10.1029/2007JF000893, 2008.

Baum, R. L., Godt, J. W., and Savage, W. Z.: Estimating the timing and location of shallow rainfall-induced landslides using a model for transient, unsaturated infiltration, Journal of Geophysical Research, 115, F03 013, https://doi.org/10.1029/2009JF001321, 2010.

Beaumont, C., Fullsack, P., and Hamilton, J.: Erosional control of active compressional orogens, in: Thrust Tectonics, pp. 1–18, Springer Netherlands, Dordrecht, https://doi.org/10.1007/978-94-011-3066-0_1, 1992.

Beer, A. R., Turowski, J. M., and Kirchner, J. W.: Spatial patterns of erosion in a bedrock gorge, Journal of Geophysical Research: Earth Surface, 122, 191–214, https://doi.org/10.1002/2016JF003850, 2017.

Beven, K. and Freer, J.: Equifinality, data assimilation, and uncertainty estimation in mechanistic modelling of complex environmental systems using the GLUE methodology, Journal of Hydrology, 249, 11–29, https://doi.org/10.1016/S0022-1694(01)00421-8, 2001.

Broeckx, J., Rossi, M., Lijnen, K., Campforts, B., Poesen, J., and Vanmaercke, M.: Landslide mobilization rates: A global analysis and model, Earth-Science Reviews, 201, 102 972, https://doi.org/10.1016/j.earscirev.2019.102972, 2020.

Burbank, D., Meigs, A., and Brozović, N.: Interactions of growing folds and coeval depositional systems, Basin Research, 8, 199–223, https://doi.org/10.1046/j.1365-2117.1996.00181.x, 1996.

Burbank, D. W.: Rates of erosion and their implications for exhumation, Mineralogical Magazine, 66, 25–52, https://doi.org/10.1180/0026461026610014, 2002.

Burbank, D. W. and Anderson, R. S.: Tectonic Geomorphology, John Wiley & Sons, Ltd, Chichester, UK, https://doi.org/10.1002/9781444345063, 2011.

Campforts, B. and Govers, G.: Keeping the edge: A numerical method that avoids knickpoint smearing when solving the stream power law, Journal of Geophysical Research: Earth Surface, 120, 1189–1205, https://doi.org/10.1002/2014JF003376, 2015.

Campforts, B., Vanacker, V., Vanderborght, J., Baken, S., Smolders, E., and Govers, G.: Simulating the mobility of meteoric 10 Be in the landscape through a coupled soil-hillslope model (Be2D), Earth and Planetary Science Letters, 439, 143–157, https://doi.org/10.1016/j.epsl.2016.01.017, 2016.

Campforts, B., Schwanghart, W., and Govers, G.: Accurate simulation of transient landscape evolution by eliminating numerical diffusion: the TTLEM 1.0 model, Earth Surface Dynamics, 5, 47–66, https://doi.org/10.5194/esurf-5-47-2017, 2017.

Campforts, B., Vanacker, V., Herman, F., Vanmaercke, M., Schwanghart, W., Tenorio, G. E., Willems, P., and Govers, G.: Parameterization of river incision models requires accounting for environmental heterogeneity: insights from the tropical Andes, Earth Surface Dynamics, 2020, 447–470, https://doi.org/10.5194/esurf-8-447-2020, 2020.

Carretier, S., Martinod, P., Reich, M., and Godderis, Y.: Modelling sediment clasts transport during landscape evolution, Earth Surface Dynamics, 4, 237–251, https://doi.org/10.5194/esurf-4-237-2016, 2016.

Carretier, S., Tolorza, V., Regard, V., Aguilar, G., Bermúdez, M. A., Martinod, J., Guyot, J. L., Hérail, G., and Riquelme, R.: Review of erosion dynamics along the major N-S climatic gradient in Chile and perspectives, Geomorphology, 300, 45–68, https://doi.org/10.1016/j.geomorph.2017.10.016, 2018.

Champel, B.: Growth and lateral propagation of fault-related folds in the Siwaliks of western Nepal: Rates, mechanisms, and geomorphic signature, Journal of Geophysical Research, 107, 2111, https://doi.org/10.1029/2001JB000578, 2002.

Claessens, L., Schoorl, J., and Veldkamp, A.: Modelling the location of shallow landslides and their effects on landscape dynamics in large watersheds: An application for Northern New Zealand, Geomorphology, 87, 16–27, https://doi.org/10.1016/j.geomorph.2006.06.039, 2007.

Cook, K. L., Turowski, J. M., and Hovius, N.: A demonstration of the importance of bedload transport for fluvial bedrock erosion and knickpoint propagation, Earth Surface Processes and Landforms, 38, 683–695, https://doi.org/10.1002/esp.3313, 2013.

Coulthard, T. J., Neal, J. C., Bates, P. D., Ramirez, J., de Almeida, G. A. M., and Hancock, G. R.: Integrating the LISFLOOD-FP 2D hydrodynamic model with the CAESAR model: implications for modelling landscape evolution, Earth Surface Processes and Landforms, 38, 1897–1906, https://doi.org/10.1002/esp.3478, 2013.

Croissant, T., Lague, D., Steer, P., and Davy, P.: Rapid post-seismic landslide evacuation boosted by dynamic river width, Nature Geoscience, 10, 680–684, https://doi.org/10.1038/ngeo3005, 2017.

Croissant, T., Steer, P., Lague, D., Davy, P., Jeandet, L., and Hilton, R. G.: Seismic cycles, earthquakes, landslides and sediment fluxes: Linking tectonics to surface processes using a reduced-complexity model, Geomorphology, 339, 87–103, https://doi.org/10.1016/j.geomorph.2019.04.017, 2019.

Culmann, K. .: Die Graphische Statike, Verlag von Meyer & Zeller, Zurich, 1875.

Dahlquist, M. P., West, A. J., and Li, G.: Landslide-driven drainage divide migration, Geology, 46, 403–406, https://doi.org/10.1130/G39916.1, 2018.

Davy, P. and Lague, D.: Fluvial erosion/transport equation of landscape evolution models revisited, Journal of Geophysical Research: Solid Earth, 114, 1–16, https://doi.org/10.1029/2008JF001146, 2009.

Davy, P., Croissant, T., and Lague, D.: A precipiton method to calculate river hydrodynamics, with applications to flood prediction, landscape evolution models, and braiding instabilities, Journal of Geophysical Research: Earth Surface, 122, 1491–1512, https://doi.org/10.1002/2016JF004156, 2017.

Densmore, A. L., Ellis, M. A., and Anderson, R. S.: Landsliding and the evolution of normal-fault-bounded mountains, Journal of Geophysical Research: Solid Earth, 103, 15 203–15 219, https://doi.org/10.1029/98JB00510, 1998.

DiBiase, R. A. and Whipple, K. X.: The influence of erosion thresholds and runoff variability on the relationships among topography, climate, and erosion rate, Journal of Geophysical Research, 116, F04 036, https://doi.org/10.1029/2011JF002095, 2011.

Dussauge, C., Grasso, J.-R., and Helmstetter, A.: Statistical analysis of rockfall volume distributions: Implications for rockfall dynamics, Journal of Geophysical Research: Solid Earth, 108, https://doi.org/10.1029/2001JB000650, http://doi.wiley.com/10.1029/2001JB000650, 2003.

Egholm, D. L., Knudsen, M. F., and Sandiford, M.: Lifespan of mountain ranges scaled by feedbacks between landsliding and erosion by rivers, Nature, 498, 475–478, https://doi.org/10.1038/nature12218, 2013.

Fan, L., Lehmann, P., McArdell, B., and Or, D.: Linking rainfall-induced landslides with debris flows runout patterns towards catchment scale hazard assessment, Geomorphology, 280, 1–15, https://doi.org/10.1016/j.geomorph.2016.10.007, 2017.

Fan, X., Scaringi, G., Korup, O., West, A. J., Westen, C. J., Tanyas, H., Hovius, N., Hales, T. C., Jibson, R. W., Allstadt, K. E., Zhang, L., Evans, S. G., Xu, C., Li, G., Pei, X., Xu, Q., and Huang, R.: Earthquake-Induced Chains of Geologic Hazards: Patterns, Mechanisms, and Impacts, Reviews of Geophysics, 57, 421–503, https://doi.org/10.1029/2018RG000626, 2019.

Farr, T. G., Rosen, P. A., Caro, E., Crippen, R., Duren, R., Hensley, S., Kobrick, M., Paller, M., Rodriguez, E., Roth, L., Seal, D., Shaffer, S., Shimada, J., Umland, J., Werner, M., Oskin, M., Burbank, D., and Alsdorf, D.: The Shuttle Radar Topography Mission, Reviews of Geophysics, 45, RG2004, https://doi.org/10.1029/2005RG000183, 2007.

Ferrier, K. L., Huppert, K. L., and Perron, J. T.: Climatic control of bedrock river incision, Nature, 496, 206–209, https://doi.org/10.1038/nature11982, 2013.

Finnegan, N. J., Hallet, B., Montgomery, D. R., Zeitler, P. K., Stone, J. O., Anders, A. M., and Yuping, L.: Coupling of rock uplift and river incision in the Namche Barwa-Gyala Peri massif, Tibet, Geological Society of America Bulletin, 120, 142–155, https://doi.org/10.1130/B26224.1, 2008.

Furbish, D. J. and Roering, J. J.: Sediment disentrainment and the concept of local versus nonlocal transport on hillslopes, Journal of Geophysical Research: Earth Surface, 118, 937–952, https://doi.org/10.1002/jgrf.20071, 2013.

Gallen, S. F., Clark, M. K., and Godt, J. W.: Coseismic landslides reveal near-surface rock strength in a high-relief, tectonically active setting, Geology, 43, 11–14, https://doi.org/10.1130/G36080.1, 2015.

Gasparini, N. M., Whipple, K. X., and Bras, R. L.: Predictions of steady state and transient landscape morphology using sediment-flux-dependent river incision models, Journal of Geophysical Research, 112, F03S09, https://doi.org/10.1029/2006JF000567, 2007.

George, D. L.: Adaptive finite volume methods with well-balanced Riemann solvers for modeling floods in rugged terrain: Application to the Malpasset dam-break flood (France, 1959), International Journal for Numerical Methods in Fluids, 66, 1000–1018, https://doi.org/10.1002/fld.2298, 2011.

Glade, R. C., Shobe, C. M., Anderson, R. S., and Tucker, G. E.: Canyon shape and erosion dynamics governed by channel-hillslope feedbacks, Geology, 47, 650–654, https://doi.org/10.1130/G46219.1, 2019.

Guns, M. and Vanacker, V.: Shifts in landslide frequency-area distribution after forest conversion in the tropical Andes, Anthropocene, 6, 75–85, https://doi.org/10.1016/j.ancene.2014.08.001, 2014.

Guzzetti, F., Malamud, B. D., Turcotte, D. L., and Reichenbach, P.: Power-law correlations of landslide areas in central Italy, Earth and Planetary Science Letters, 195, 169–183, https://doi.org/10.1016/S0012-821X(01)00589-1, 2002.

Guzzetti, F., Reichenbach, P., Ardizzone, F., Cardinali, M., and Galli, M.: Estimating the quality of landslide susceptibility models, Geomorphology, 81, 166–184, https://doi.org/10.1016/j.geomorph.2006.04.007, 2006.

Hancock, G. S. and Anderson, R. S.: Numerical modeling of fluvial strath-terrace formation in response to oscillating climate, Bulletin of the Geological Society of America, https://doi.org/10.1130/0016-7606(2002)114<1131:NMOFST>2.0.CO, 2002.

Hobley, D. E., Sinclair, H. D., Mudd, S. M., and Cowie, P. A.: Field calibration of sediment flux dependent river incision, Journal of Geophysical Research: Earth Surface, 116, F04 017, https://doi.org/10.1029/2010JF001935, 2011.

Horton, P., Jaboyedoff, M., Rudaz, B., and Zimmermann, M.: Flow-R, a model for susceptibility mapping of debris flows and other gravitational hazards at a regional scale, Natural Hazards and Earth System Sciences, 13, 869–885, https://doi.org/10.5194/nhess-13-869-2013, 2013.

Hovius, N., Stark, C. P., and Allen, P. A.: Sediment flux from a mountain belt derived by landslide mapping, Geology, 25, 231–234, https://doi.org/10.1130/0091-7613(1997)025<0231:SFFAMB>2.3.CO;2, 1997.

Hovius, N., Stark, C. P., Hao-Tsu, C., and Jiun-Chuan, L.: Supply and Removal of Sediment in a Landslide-Dominated Mountain Belt: Central Range, Taiwan, The Journal of Geology, 108, 73–89, https://doi.org/10.1086/314387, 2000.

Hovius, N., Meunier, P., Lin, C. W., Chen, H., Chen, Y. G., Dadson, S., Horng, M. J., and Lines, M.: Prolonged seismically induced erosion and the mass balance of a large earthquake, Earth and Planetary Science Letters, 304, 347–355, https://doi.org/10.1016/j.epsl.2011.02.005, 2011.

Howard, A. D. and Kerby, G.: Channel changes in badlands, Geological Society of America Bulletin, 94, 739, https://doi.org/10.1130/0016-7606(1983)94<739:CCIB>2.0.CO;2, 1983.

Iverson, R. M.: Landslide triggering by rain infiltration, Water Resources Research, 36, 1897–1910, https://doi.org/10.1029/2000WR900090, 2000.

Iverson, R. M. and George, D. L.: Modelling landslide liquefaction, mobility bifurcation and the dynamics of the 2014 Oso disaster, Géotechnique, 66, 175–187, https://doi.org/10.1680/jgeot.15.LM.004, 2016.

Jeandet, L., Steer, P., Lague, D., and Davy, P.: Coulomb Mechanics and Relief Constraints Explain Landslide Size Distribution, Geophysical Research Letters, 46, 4258–4266, https://doi.org/10.1029/2019GL082351, 2019.

Kean, J. W. and Smith, J. D.: Flow and boundary shear stress in channels with woody bank vegetation, Riparian Vegetation and Fluvial Geomorphology, 8, 237–252, https://doi.org/10.1029/008WSA17, 2004.

Keefer, D. K.: Landslides caused by earthquakes, Geological Society of America Bulletin, 95, 406, https://doi.org/10.1130/0016-7606(1984)95<406:LCBE>2.0.CO;2, 1984.

Keefer, D. K.: Investigating landslides caused by earthquakes - A historical review, Surveys in Geophysics, 23, 473–510, https://doi.org/10.1023/A:1021274710840, 2002.

Keefer, D. K. and Larsen, M. C.: Assessing Landslide Hazards, Science, 316, 1136–1138, https://doi.org/10.1126/science.1143308, 2007.

King, G. E., Herman, F., Lambert, R., Valla, P. G., and Guralnik, B.: Multi-OSL-thermochronometry of feldspar, Quaternary Geochronology, 33, 76–87, https://doi.org/10.1016/j.quageo.2016.01.004, 2016.

Kirby, E. and Whipple, K. X.: Expression of active tectonics in erosional landscapes, Journal of Structural Geology, 44, 54–75, https://doi.org/10.1016/j.jsg.2012.07.009, 2012.

Korup, O.: Large landslides and their effect on sediment flux in South Westland, New Zealand, Earth Surface Processes and Landforms, 30, 305–323, https://doi.org/10.1002/esp.1143, 2005.

Korup, O.: Rock type leaves topographic signature in landslide-dominated mountain ranges, Geophysical Research Letters, 35, L11 402, https://doi.org/10.1029/2008GL034157, 2008.

Korup, O., Clague, J. J., Hermanns, R. L., Hewitt, K., Strom, A. L., and Weidinger, J. T.: Giant landslides, topography, and erosion, Earth and Planetary Science Letters, 261, 578–589, https://doi.org/10.1016/j.epsl.2007.07.025, 2007.

Korup, O., Densmore, A. L., and Schlunegger, F.: The role of landslides in mountain range evolution, Geomorphology, https://doi.org/10.1016/j.geomorph.2009.09.017, 2010.

Lague, D.: Reduction of long-term bedrock incision efficiency by short-term alluvial cover intermittency, Journal of Geophysical Research: Earth Surface, 115, n/a–n/a, https://doi.org/10.1029/2008JF001210, 2010.

Lague, D.: The stream power river incision model: evidence, theory and beyond, Earth Surface Processes and Landforms, 39, 38–61, https://doi.org/10.1002/esp.3462, 2014.

Lague, D., Hovius, N., and Davy, P.: Discharge, discharge variability, and the bedrock channel profile, Journal of Geophysical Research: Earth Surface, 110, n/a–n/a, https://doi.org/10.1029/2004JF000259, 2005.

Larsen, I. J. and Montgomery, D. R.: Landslide erosion coupled to tectonics and river incision, Nature Geoscience, 5, 468–473, https://doi.org/10.1038/ngeo1479, 2012.

Larsen, I. J., Montgomery, D. R., and Korup, O.: Landslide erosion controlled by hillslope material, Nature Geoscience, 3, 247–251, https://doi.org/10.1038/ngeo776, 2010.

Li, G., West, A. J., Densmore, A. L., Hammond, D. E., Jin, Z., Zhang, F., Wang, J., and Hilton, R. G.: Connectivity of earthquake-triggered landslides with the fluvial network: Implications for landslide sediment transport after the 2008 Wenchuan earthquake, Journal of Geophysical Research: Earth Surface, 121, 703–724, https://doi.org/10.1002/2015JF003718, 2016.

Lin, G.-W., Chen, H., Chen, Y.-H., and Horng, M.-J.: Influence of typhoons and earthquakes on rainfall-induced landslides and suspended sediments discharge, Engineering Geology, 97, 32–41, https://doi.org/10.1016/j.enggeo.2007.12.001, 2008.

Malamud, B. D. and Turcotte, D. L.: Self-organized criticality applied to natural hazards, in: Natural Hazards, vol. 20, pp. 93–116, https://doi.org/10.1023/A:1008014000515, 1999.

Malamud, B. D., Turcotte, D. L., Guzzetti, F., and Reichenbach, P.: Landslide inventories and their statistical properties, Earth Surface Processes and Landforms, 29, 687–711, https://doi.org/10.1002/esp.1064, 2004.

Marc, O., Hovius, N., Meunier, P., Uchida, T., and Hayashi, S.: Transient changes of landslide rates after earthquakes, Geology, 43, 883–886, https://doi.org/10.1130/G36961.1, 2015.

Marc, O., Stumpf, A., Malet, J.-P., Gosset, M., Uchida, T., and Chiang, S.-H.: Initial insights from a global database of rainfall-induced landslide inventories: the weak influence of slope and strong influence of total storm rainfall, Earth Surface Dynamics, 6, 903–922, https://doi.org/10.5194/esurf-6-903-2018, 2018.

Marc, O., Behling, R., Andermann, C., Turowski, J. M., Illien, L., Roessner, S., and Hovius, N.: Long-term erosion of the Nepal Himalayas by bedrock landsliding: The role of monsoons, earthquakes and giant landslides, Earth Surface Dynamics, 7, 107–128, https://doi.org/10.5194/esurf-7-107-2019, 2019.

Meunier, P., Hovius, N., and Haines, A. J.: Regional patterns of earthquake-triggered landslides and their relation to ground motion, Geophysical Research Letters, 34, L20 408, https://doi.org/10.1029/2007GL031337, 2007.

Milliman, J. D. and Meade, R. H.: World-Wide Delivery of River Sediment to the Oceans, The Journal of Geology, https://doi.org/10.1086/628741, 1983.

Montgomery, D. R. and Dietrich, W. E.: A physically based model for the topographic control on shallow landsliding, Water Resources Research, 30, 1153–1171, https://doi.org/10.1029/93WR02979, 1994.

Montgomery, D. R. and Gran, K. B.: Downstream variations in the width of bedrock channels, Water Resources Research, 37, 1841–1846, https://doi.org/10.1029/2000WR900393, 2001.

Mudd, S. M.: Detection of transience in eroding landscapes, Earth Surface Processes and Landforms, 42, 24–41, https://doi.org/10.1002/esp.3923, 2017.

Niemi, N. A., Oskin, M., Burbank, D. W., Heimsath, A. M., and Gabet, E. J.: Effects of bedrock landslides on cosmogenically determined erosion rates, Earth and Planetary Science Letters, 237, 480–498, https://doi.org/10.1016/j.epsl.2005.07.009, 2005.

Ouimet, W. B., Whipple, K. X., Royden, L. H., Sun, Z., and Chen, Z.: The influence of large landslides on river incision in a transient landscape: Eastern margin of the Tibetan Plateau (Sichuan, China), Geological Society of America Bulletin, 119, 1462–1476, https://doi.org/10.1130/B26136.1, 2007.

Ouimet, W. B., Whipple, K. X., Crosby, B. T., Johnson, J. P., and Schildgen, T. F.: Epigenetic gorges in fluvial landscapes, Earth Surface Processes and Landforms, 33, 1993–2009, https://doi.org/10.1002/esp.1650, 2008.

Page, M. J., Reid, L. M., and Lynn, I. H.: New Zealand Hydrological Society Sediment production from Cyclone Bola landslides, Waipaoa catchment, Source Journal of Hydrology (New Zealand), 38, 289–308, 1999.

Paola, C. and Voller, V. R.: A generalized Exner equation for sediment mass balance, Journal of Geophysical Research: Earth Surface, 110, 1–8, https://doi.org/10.1029/2004JF000274, 2005.

Parker, R. N., Hales, T. C., Mudd, S. M., Grieve, S. W. D., and Constantine, J. A.: Colluvium supply in humid regions limits the frequency of storm-triggered landslides, Scientific Reports, 6, 34 438, https://doi.org/10.1038/srep34438, 2016.

Pelletier, J. D.: Minimizing the grid-resolution dependence of flow-routing algorithms for geomorphic applications, Geomorphology, 122, 91–98, https://doi.org/10.1016/j.geomorph.2010.06.001, 2010.

Roback, K., Clark, M. K., West, A. J., Zekkos, D., Li, G., Gallen, S. F., Chamlagain, D., and Godt, J. W.: The size, distribution, and mobility of landslides caused by the 2015 Mw7.8 Gorkha earthquake, Nepal, Geomorphology, 301, 121–138, https://doi.org/10.1016/j.geomorph.2017.01.030, 2018.

Robinson, T. R., Rosser, N. J., Densmore, A. L., Williams, J. G., Kincey, M. E., Benjamin, J., and Bell, H. J. A.: Rapid post-earthquake modelling of coseismic landslide intensity and distribution for emergency response decision support, Natural Hazards and Earth System Sciences, 17, 1521–1540, https://doi.org/10.5194/nhess-17-1521-2017, 2017.

Roering, J. J., Kirchner, J. W., and Dietrich, W. E.: Evidence for nonlinear, diffusive sediment transport on hillslopes and implications for landscape morphology, Water Resources Research, 35, 853–870, https://doi.org/10.1029/1998WR900090, 1999.

Scherler, D., DiBiase, R. A., Fisher, G. B., and Avouac, J.-P.: Testing monsoonal controls on bedrock river incision in the Himalaya and Eastern Tibet with a stochastic-threshold stream power model, Journal of Geophysical Research: Earth Surface, 122, 1389–1429, https://doi.org/10.1002/2016JF004011, 2017.

Schwanghart, W. and Scherler, D.: Short Communication: TopoToolbox 2 - MATLAB-based software for topographic analysis and modeling in Earth surface sciences, Earth Surface Dynamics, 2, 1–7, https://doi.org/10.5194/esurf-2-1-2014, 2014.

Schwanghart, W., Bernhardt, A., Stolle, A., Hoelzmann, P., Adhikari, B. R., Andermann, C., Tofelde, S., Merchel, S., Rugel, G., Fort, M., and Korup, O.: Repeated catastrophic valley infill following medieval earthquakes in the Nepal Himalaya, Science, 351, 147–150, https://doi.org/10.1126/science.aac9865, 2016.

Seidl, M. A. and Dietrich, W. E.: The problem of channel erosion into bedrock, Catena Supplement, 23, 101–124, 1992.

Shobe, C. M., Tucker, G. E., and Anderson, R. S.: Hillslope-derived blocks retard river incision, Geophysical Research Letters, 43, 5070–5078, https://doi.org/10.1002/2016GL069262, 2016.

Shobe, C. M., Tucker, G. E., and Barnhart, K. R.: The SPACE 1.0 model: a Landlab component for 2-D calculation of sediment transport, bedrock erosion, and landscape evolution, Geoscientific Model Development, 10, 4577–4604, https://doi.org/10.5194/gmd-10-4577-2017, https://www.geosci-model-dev.net/10/4577/2017/, 2017.

Shobe, C. M., Tucker, G. E., and Rossi, M. W.: Variable-Threshold Behavior in Rivers Arising From Hillslope-Derived Blocks, Journal of Geophysical Research: Earth Surface, 123, 1931–1957, https://doi.org/10.1029/2017JF004575, 2018.

Sidle, R. C. and Ochiai, H.: Landslides: Processes, Prediction, and Land Use, Water Resources Monograph, American Geophysical Union, Washington, D. C., https://doi.org/10.1029/WM018, 2006.

Sklar, L. S. and Dietrich, W. E.: A mechanistic model for river incision into bedrock by saltating bed load, Water Resources Research, 40, W06 301, https://doi.org/10.1029/2003WR002496, 2004.

Snyder, N. P., Whipple, K. X., Tucker, G. E., and Merritts, D. J.: Importance of a stochastic distribution of floods and erosion thresholds in the bedrock river incision problem, Journal of Geophysical Research: Solid Earth, 108, 2388, https://doi.org/10.1029/2001JB001655, 2003.

Stark, C. P. and Hovius, N.: The characterization of landslide size distributions, Geophysical Research Letters, 28, 1091–1094, https://doi.org/10.1029/2000GL008527, 2001.

Taylor, D.: Fundamentals of Soil Mechanics, Wiley, New York, 1948.

Tenorio, G. E., Vanacker, V., Campforts, B., Álvarez, L., Zhiminaicela, S., Vercruysse, K., Molina, A., and Govers, G.: Tracking spatial variation in river load from Andean highlands to inter-Andean valleys, Geomorphology, 308, 175–189, https://doi.org/10.1016/j.geomorph.2018.02.009, 2018.

Tucker, G. E.: Drainage basin sensitivity to tectonic and climatic forcing: Implications of a stochastic model for the role of entrainment and erosion thresholds, Earth Surface Processes and Landforms, 29, 185–205, https://doi.org/10.1002/esp.1020, 2004.

Tucker, G. E. and Hancock, G. R.: Modelling landscape evolution, Earth Surface Processes and Landforms, 35, 28–50, https://doi.org/10.1002/esp.1952, 2010.

Turowski, J. M., Lague, D., and Hovius, N.: Cover effect in bedrock abrasion: A new derivation and its implications for the modeling of bedrock channel morphology, Journal of Geophysical Research, 112, F04 006, https://doi.org/10.1029/2006JF000697, 2007.

Turowski, J. M., Lague, D., and Hovius, N.: Response of bedrock channel width to tectonic forcing: Insights from a numerical model, theoretical considerations, and comparison with field data, Journal of Geophysical Research, 114, F03 016, https://doi.org/10.1029/2008JF001133, 2009.

Van Asch, T., Buma, J., and Van Beek, L.: A view on some hydrological triggering systems in landslides, Geomorphology, 30, 25–32, https://doi.org/10.1016/S0169-555X(99)00042-2, 1999.

Van Rompaey, A. J. J. and Govers, G.: Data quality and model complexity for regional scale soil erosion prediction, International Journal of Geographical Information Science, 16, 663–680, https://doi.org/10.1080/13658810210148561, 2002.

Wang, J., Jin, Z., Hilton, R. G., Zhang, F., Densmore, A. L., Li, G., and West, A. J.: Controls on fluvial evacuation of sediment from earthquake-triggered landslides, Geology, 43, 115–118, https://doi.org/10.1130/G36157.1, 2015.

Wang, W., Godard, V., Liu-Zeng, J., Scherler, D., Xu, C., Zhang, J., Xie, K., Bellier, O., Ansberque, C., and de Sigoyer, J.: Perturbation of fluvial sediment fluxes following the 2008 Wenchuan earthquake, Earth Surface Processes and Landforms, 42, 2611–2622, https://doi.org/10.1002/esp.4210, 2017.

Whipple, K. X. and Tucker, G. E.: Dynamics of the stream-power river incision model: Implications for height limits of mountain ranges, landscape response timescales, and research needs, Journal of Geophysical Research: Solid Earth, 104, 17 661–17 674, https://doi.org/10.1029/1999JB900120, 1999.

Whipple, K. X., Hancock, G. S., and Anderson, R. S.: River incision into bedrock: Mechanics and relative efficacy of plucking, abrasion, and cavitation, Geological Society of America Bulletin, 112, 490–503, https://doi.org/10.1130/0016-7606(2000)112<490:RIIBMA>2.0.CO;2, 2000.

Willgoose, G., Bras, R. L., and Rodrigueziturbe, I.: Results from a New Model of River Basin Evolution, Earth Surface Processes and Landforms, 16, 237–254, https://doi.org/10.1002/esp.3290160305, 1991.

Wobus, C., Whipple, K. X., Kirby, E., Snyder, N., Johnson, J., Spyropolou, K., Crosby, B., and Sheehan, D.: Tectonics from topography: Procedures, promise, and pitfalls, in: Tectonics, Climate, and Landscape Evolution, vol. 398, pp. 55–74, Geological Society of America, https://doi.org/10.1130/2006.2398(04), 2006.

Wyllie, D. C. and Mah, C. W.: Rock Slope Engineering, CRC Press, https://doi.org/10.1201/9781315274980, 2017.

Yanites, B. J.: The Dynamics of Channel Slope, Width, and Sediment in Actively Eroding Bedrock River Systems, Journal of Geophysical Research: Earth Surface, 123, 1504–1527, https://doi.org/10.1029/2017JF004405, 2018.

Yanites, B. J., Tucker, G. E., and Anderson, R. S.: Numerical and analytical models of cosmogenic radionuclide dynamics in landslide-dominated drainage basins, Journal of Geophysical Research, 114, F01 007, https://doi.org/10.1029/2008JF001088, 2009.

Zhang, J., J Van Westen, C., Tanyas, H., Mavrouli, O., Ge, Y., Bajrachary, S., Raj Gurung, D., Raj Dhital, M., and Raj Khanal, N.: How size and trigger matter: Analyzing rainfall- A nd earthquake-triggered landslide inventories and their causal relation in the Koshi River basin, central Himalaya, Natural Hazards and Earth System Sciences, 19, 1789–1805, https://doi.org/10.5194/nhess-19-1789-2019, 2019.

Zhang, L., Stark, C., Schumer, R., Kwang, J., Li, T., Fu, X., Wang, G., and Parker, G.: The Advective-Diffusive Morphodynamics of Mixed Bedrock-Alluvial Rivers Subjected to Spatiotemporally Varying Sediment Supply, Journal of Geophysical Research: Earth Surface, 123, 1731–1755, https://doi.org/10.1029/2017JF004431, 2018.

Zhou, S., Ouyang, C., An, H., Jiang, T., and Xu, Q.: Comprehensive study of the Beijing Daanshan rockslide based on real-time videos, field investigations, and numerical modeling, Landslides, https://doi.org/10.1007/s10346-020-01345-2, 2020.

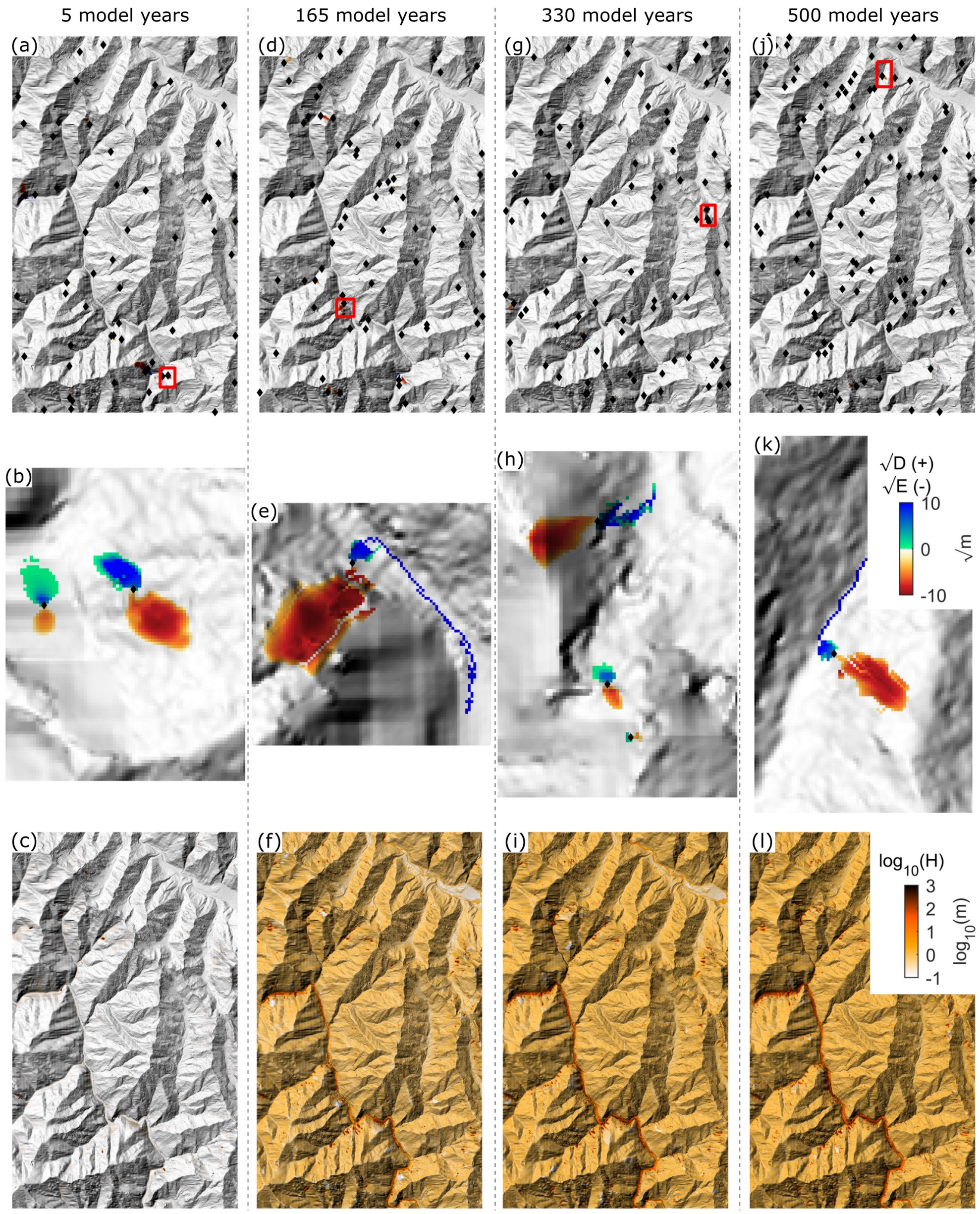

Figure 7. ~~Timeslices of HyLands model run for the Namche Barwa region after 5, 165, 330 and 500 model years~~**Timeslices of HyLands model run for the Namche Barwa-Gyala Peri massif after 5, 165, 330 and 500 model years**. (**a, d, g, j**) Indicate the location of the landslides at the given timestep (black ~~dots~~diamonds). (**b, e, h, k**) Zoom into the red squares on (a, d, g and j) showing simulated landslide erosion/deposition. The colors represent the square root (~~used~~ for ease of visualization) of ~~the~~ landslide erosion (-) and deposition (+) during the ~~given~~ presented time step. ~~(**b, e, h, k**) Zoom of simulated landslide erosion/deposition indicated with the red square in respectively (a, d, g and j).~~ (**c, f, i, l**) ~~Represent~~ show the ~~square root of the total amount of~~ sediment thickness, H, generated through river incision (SPACE module) and landsliding~~after respectively 5, 500, 1500 and 2000 model years~~. The ~~grey shaded colours indicate elevations, which were~~ underlying hillshade was derived from the 30 m SRTM v3 DEM ~~(?)~~(Farr et al., 2007).

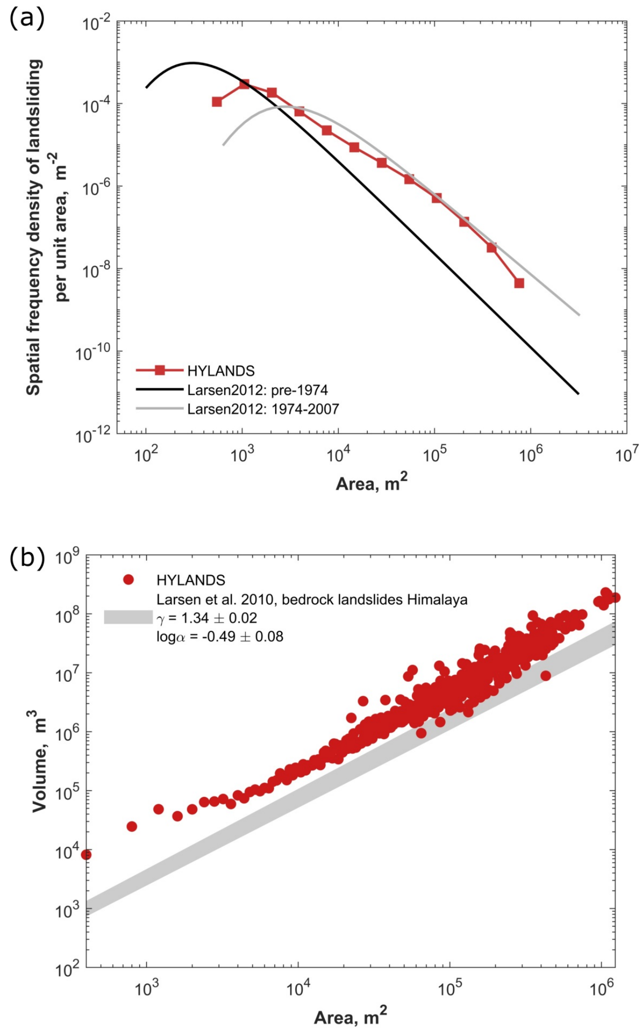

Figure 8. Comparison between modelled and observed characteristic landslide scaling relationships. (**a**) ~~Magnitude frequency~~ Magnitude-frequency relationship. The grey and black ~~line~~ lines represent the best fitting inverse gamma distribution (Eq. 19) of the landslide activity mapped before 1974 and between 1974 - 2012, respectively (Larsen and Montgomery, 2012). The fitting parameters are respectively ($a_l = 768 \times 10^{-6}$, $s_l = -32.6 \times 10^{-6}$ and $\rho_l = 1.27$) and ($a_l = 6100 \times 10^{-6}$, $s_l = -311 \times 10^{-6}$ and $\rho_l = 0.96$)). The red dots represent the magnitude-frequency distribution simulated using HyLands. (**b**) Area-Volume relationship. The grey dashed zone represents the expected area-volume scaling relationship, observed for bedrock landslides in the Himalaya (Larsen et al., 2010). Fit is calculated using Eq. 20 with fitting parameters $\gamma = 1.32 \pm 0.02$ and ${}^{10}\log\alpha = -0.49 \pm 0.06$. The red dots represent the geometry of the ~~data~~ landslides simulated with HyLands.

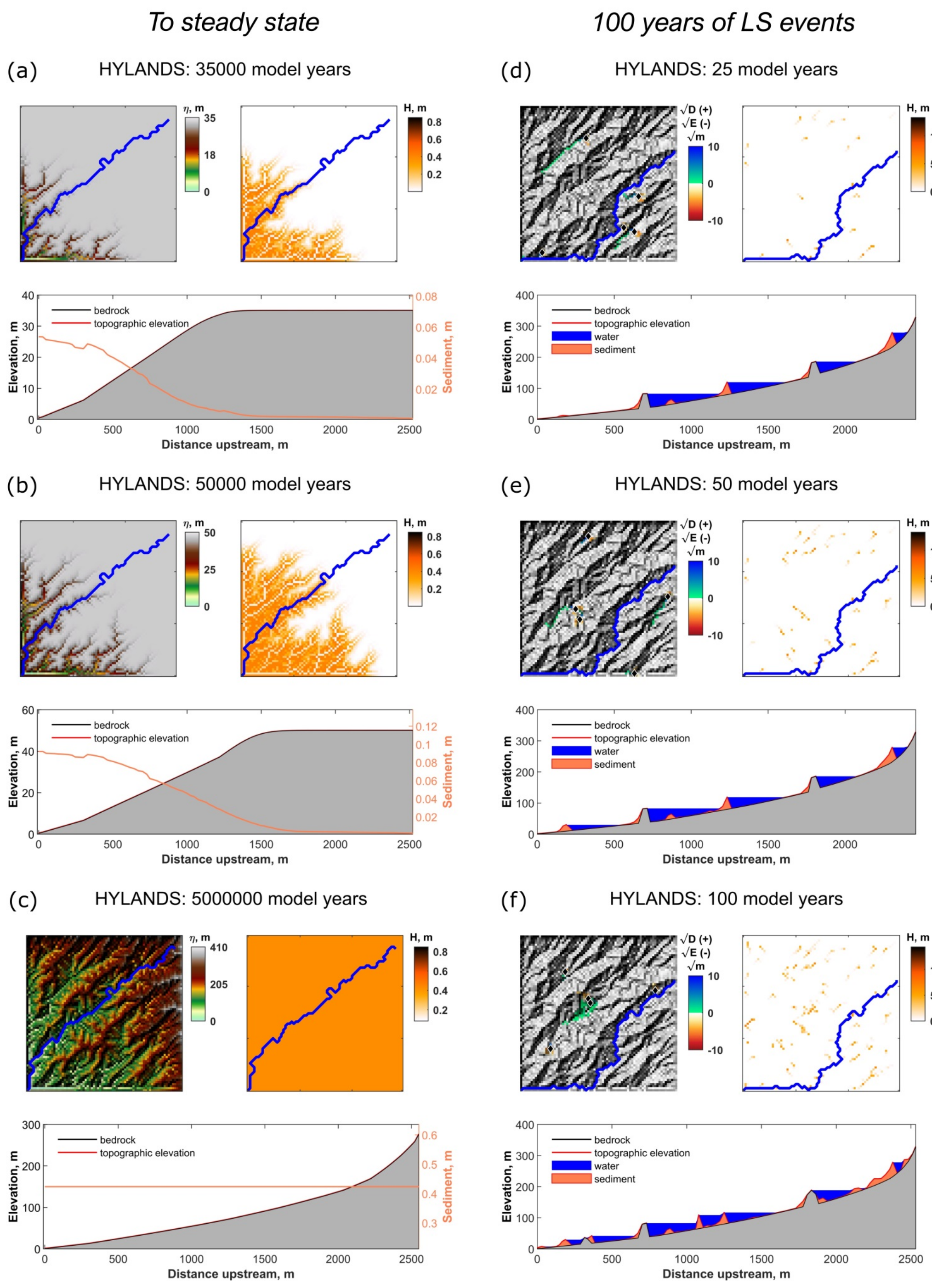

Figure 9. Synthetic model run showing landscape evolution to steady state followed by an intense landsliding period of 100 years. **(a-d)** Time slices showing evolution of the landscape to steady state, before the landslide period. **(e-h)** Time slices showing the landslide period where intense landsliding is occurring over a period of 100 years. Note that, during landsliding, both pure landslide dams arise as well as irregularities in the bedrock profile (the grey bumps). The latter originate from the river being redirected after landsliding forming epigenetic gorges (see text).

Figure 9. continued from previous page. **(a-d)** Time slices showing evolution of the landscape to steady state, before the landslide period. The upper left subplots show the evolution of topography through time. The upper right subplots show the evolution of of sediment thickness (H) through time. On both subplots, the blue line represents the location of the river plotted in the lower subplots. These lower subplots show the topographic and bedrock elevation (red and black line respectively). The difference between the topographic elevation and the elevation of the bedrock represents the sediment thickness. With respect to total elevation, sediment thickness is small, so sediment thickness (orange line) is also plotted against the right-hand y-axis. The gray shaded area represents bedrock underlying the river profile. **(e-h)** Time slices showing the landslide period where intense landsliding is occurring over a period of 100 years. The upper left subplots show the landslide activity. The location of landslides is indicated with black diamonds. The colors represent the square root of the landslide erosion (-) and deposition (+) during the presented time step. The upper right subplots show the evolution of of sediment thickness (H) through time. On both subplots, the blue line represents the location of the river plotted in the lower subplots. These lower subplots show the topographic and bedrock elevation (red and black line respectively) as well as the volume occupied by sediments and water (orange and blue shaded area respectively). Note that, during landsliding, both pure landslide dams arise as well as irregularities in the bedrock profile (the grey bumps). The latter originate from the river being redirected after landsliding, forming epigenetic gorges (see text).

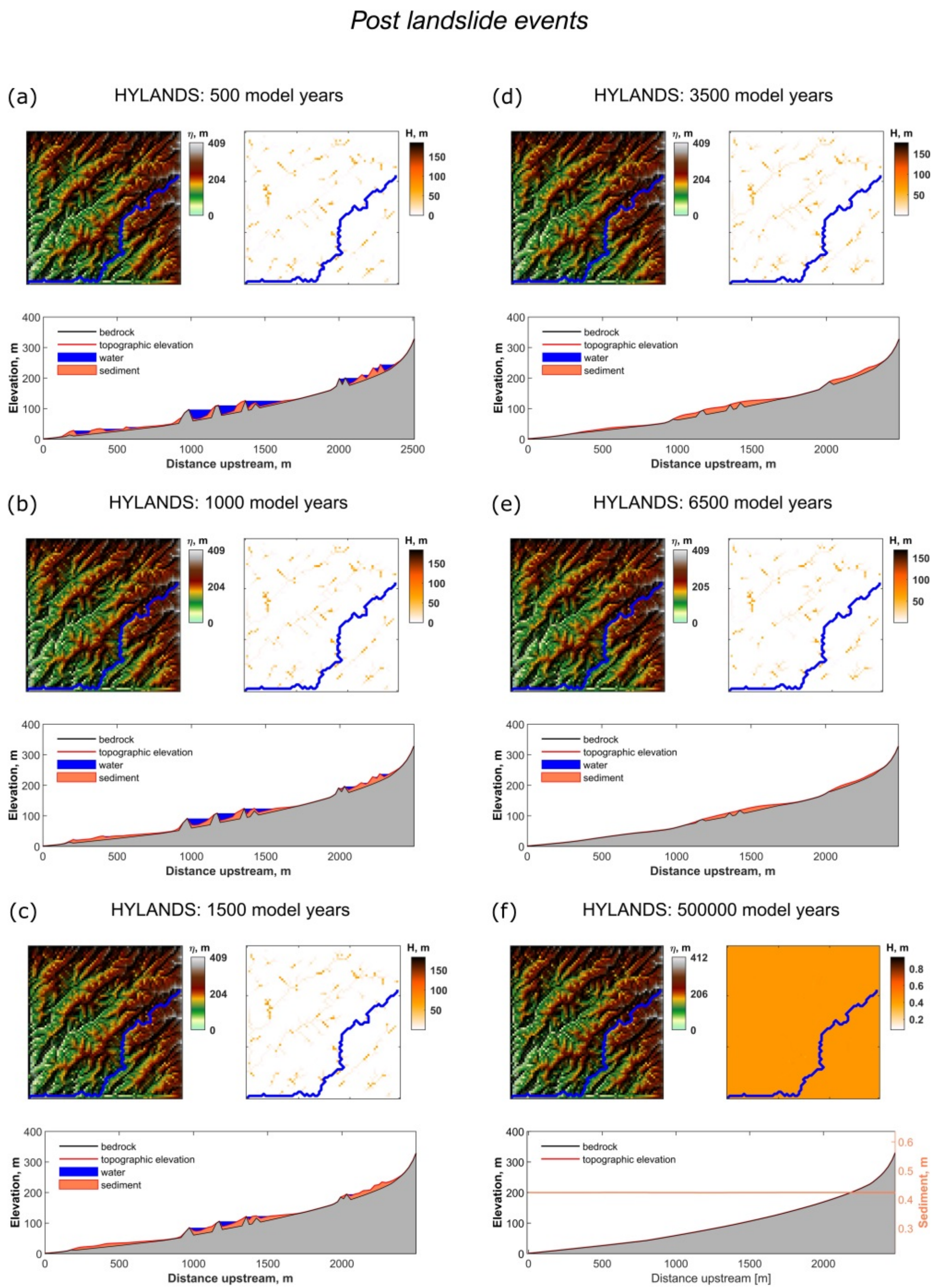

Figure 10. Synthetic model run showing recovery from intense landsliding illustrated in Fig. 9. ~~**(a-h)** Time slices showing reestablishment of the landscape steady state. Bedrock bumps created by landslide-induced drainage redirection are eroded and the channel re-attains its smoothly concave-up, steady-state configuration.~~

Figure 10. **(a-h)** Time slices showing reestablishment of the landscape to steady state. Bedrock bumps created by landslide-induced drainage redirection are eroded and the channel re-attains its smoothly concave-up, steady-state configuration. For a detailed description of subplots and labels, see Fig. 9.